

# Exhumation mechanisms of melt-bearing ultrahigh pressure crustal rocks during collision of spontaneously moving plates

E. SIZOVA,<sup>1</sup> T. GERYA<sup>1,2</sup> AND M. BROWN<sup>3</sup>

<sup>1</sup>ETH-Zurich, Institute of Geophysics, Switzerland (e-mail: sizovaev@gmail.com)

<sup>2</sup>Geology Department, Moscow State University, 119199 Moscow, Russia

<sup>3</sup>Department of Geology, University of Maryland, College Park, MD 20742, USA

**ABSTRACT** A series of 2D petrological–thermomechanical numerical experiments was conducted to: (i) characterize the variability of exhumation mechanisms of ultrahigh pressure metamorphic (UHPM) rocks during collision of spontaneously moving plates and (ii) study the possible geodynamic effects of melting at ultrahigh pressure conditions for the exhumation of high-temperature–ultrahigh pressure metamorphic (HT–UHPM) rocks. To this end, the models include fluid- and melt-induced weakening of rocks. Five distinct modes of exhumation of (U)HPM rocks associated with changes in several parameters in the models of plate collision and continent subduction are identified as follows: vertical crustal extrusion, large-scale crustal stacking, shallow crustal delamination, trans-lithospheric diapirism, and channel flow. The variation in exhumation mechanisms for (U)HPM rocks in numerical models of collision driven by spontaneously moving plates contrasts with the domination of the channel flow mode of exhumation in a majority of the published results from numerical models of collision that used a prescribed plate convergence velocity and/or did not include fluid- and melt-induced weakening of rocks. This difference in the range of exhumation mechanisms suggests that the prescribed convergence velocity condition and the neglect of fluid- and melt-related weakening effects in the earlier models may inhibit development of several important collisional processes found in our experiments, such as slab breakoff, vertical crustal extrusion, large-scale stacking, shallow crustal delamination and relamination, and eduction of the continental plate. Consequently, the significance of channel flow for the exhumation of UHPM rocks may have been overstated based on the results of the earlier numerical experiments. In addition, the results from this study extend over a larger proportion of the high-temperature range of  $P$ – $T$  conditions documented from UHPM rocks, including those retrieved from HT–UHPM rocks, than the results of experiments from previous numerical models. In particular, the highest peak metamorphic temperatures (up to 1000 °C) are recorded in the case of the vertical crustal extrusion model in which subducted continental crust is subjected to a period of prolonged heating by asthenospheric mantle abutting the continental side of the vertically hanging slab. Nonetheless, some extreme temperature conditions which have been suggested for the Kokchetav and Bohemian massifs, perhaps up to 1100–1200 °C, are still to be achieved in experiments using numerical models.

**Key words:** continental subduction; diapirism; exhumation of UHPM rocks; extrusion of HT–UHPM rocks; melting at (U)HPM.

## INTRODUCTION

Since the discovery of coesite in rocks from the Western Alps (Chopin, 1984) an increasing number of ultrahigh pressure metamorphic (UHPM) occurrences have been documented from all over the world. In multiple studies it has been shown that buoyant crustal rocks can be subducted to mantle depths of more than 100 km, experience UHP metamorphism, and then be exhumed back to lower-to-middle crustal depths where erosion or younger tectonic events are responsible for final exhumation to the surface.

To understand the mechanisms of formation and subsequent exhumation of UHPM rocks it is important to determine the structural relations of the UHPM

rock unit with the overlying and underlying rock units and the tectonic settings in which the UHPM rocks were generated. Higher-temperature UHPM rocks mostly have continental protoliths, including the continental crust and its overlying sedimentary succession (Maruyama *et al.*, 1996; Chopin, 2003), in contrast to colder, lawsonite-bearing oceanic UHPM rocks (Tsuji-mori *et al.*, 2006). The higher-temperature UHPM rocks are found within major continental collision belts and extend laterally for several hundred kilometres; most are in Eurasia, with rare examples in Africa, Central America and Antarctica. Many of the exhumed UHPM rocks exposed at the surface occur as subhorizontal sheets 1–5 km in thickness, bounded by normal faults on the top and reverse faults on the

bottom, sandwiched between HPM rocks or even lower grade metamorphic units (Kaneko *et al.*, 2000; Ernst, 2001; Liou *et al.*, 2004). Typically, these UHPM rocks now form the cores of antiformal nappe stacks that define structural domes 5–50 km across (Faure *et al.*, 2003; Xu *et al.*, 2006; Epard & Steck, 2008). The upper levels of many HPM–UHPM terranes are dominated by extensional structures formed during and/or after initial exhumation from UHPM conditions (Andersen & Jamtveit, 1990; Ratschbacher *et al.*, 2000; Avigad *et al.*, 2003).

Although the process of exhumation of HPM and UHPM rocks from mantle depths to lower-to-middle crustal depths is a hotly debated issue in the geoscience community, in general terms initial exhumation to crustal depths must be driven by either internal forces, such as the buoyancy of the subducted material, or external forces, such as the flow of the surrounding material, or some combination of these two driving forces. Examples of predominantly buoyancy-driven mechanisms include channel flow during ongoing continental subduction (e.g. Mancktelow, 1995; Dobretsov, 2000; Epard & Steck, 2008; Gerya *et al.*, 2008; Warren *et al.*, 2008a,b; Beaumont *et al.*, 2009), wedge extrusion induced by detachment of the deeply subducted crustal materials from the downgoing plate and subsequent upward motion (e.g. van den Beukel, 1992; Okay *et al.*, 1993; Ernst & Liou, 1995; Kaneko *et al.*, 2000; Smye *et al.*, 2010), and diapiric ascent of subducted continental materials (e.g. Cloos, 1993; Wang & Cong, 1999; Hacker *et al.*, 2005; Root *et al.*, 2005; Wallis *et al.*, 2005; Yin *et al.*, 2007; Behn *et al.*, 2011; Little *et al.*, 2011), and examples of mechanisms driven predominantly by external forces include large-scale intracontinental thrusting (e.g. Okay & Sengör, 1992; Okay *et al.*, 1993; Yin & Nie, 1993; Brueckner *et al.*, 2010; Hacker *et al.*, 2010; ) with coeval erosional exhumation (e.g. Nie *et al.*, 1994; Chemenda *et al.*, 1995), pure-shear crustal thickening and coeval erosional exhumation during continent–continent collision (e.g. Dewey *et al.*, 1993; Ryan, 2001), decoupling and exhumation of the continental plate (e.g. Andersen *et al.*, 1991; Duretz *et al.*, 2011) and changes in plate kinematics at the trench (e.g. Brun & Faccenna, 2008; Husson *et al.*, 2009; Li *et al.*, 2011).

Understanding the process of exhumation of HPM and UHPM rocks has been advanced by geodynamic numerical and analogue modelling (e.g. Chemenda *et al.*, 1995, 2000; Burov *et al.*, 2001; Boutelier *et al.*, 2004; Gerya *et al.*, 2008; Warren *et al.*, 2008a,b; Yamato *et al.*, 2008; Beaumont *et al.*, 2009; Li & Gerya, 2009; Butler *et al.*, 2011), but nonetheless some details in these models cannot be fully reconciled with observations from the geological record. The models predict subduction of crustal rocks to extreme depths of 150–200 km (pressure up to 5–6 GPa at maximum temperature of 600–900 °C) and exhumation back to the surface in a subduction channel associated with strong deformation and tectonic

mixing of rock units derived from different protoliths and depths – a process generally referred to channel flow (e.g. Burov *et al.*, 2001; Gerya *et al.*, 2008; Warren *et al.*, 2008a; Li & Gerya, 2009; ), which can be reconciled with some (U)HPM complexes (e.g. Beaumont *et al.*, 2009). A majority of the numerical models use a prescribed plate convergence velocity. However, a prescribed plate convergence velocity does not depend on slab pull, which is the principal driving force for subduction, and as such these models cannot account for natural changes in the driving force, whether gradual (e.g. due to progressive subduction) or abrupt (e.g. due to slab breakoff). However, studies using alternative numerical models with spontaneous plate motion driven by evolving slab pull and ridge push forces, which better mimic nature (e.g. Faccenda *et al.*, 2008; Duretz *et al.*, 2011), are insufficient in number to characterize fully the range of parameters that potentially may demonstrate the feasibility of other popular mechanisms of exhumation of UHPM rocks.

Another issue is that peak temperatures in experiments to date using numerical models have consistently failed to achieve those recorded in nature (e.g. Stoeckhert & Gerya, 2005; Warren *et al.*, 2008a,b; Yamato *et al.*, 2008). Whereas high to ultrahigh pressures are achieved in a majority of these experiments, maximal temperatures are generally >100 °C lower than those retrieved from high temperature–ultrahigh pressure metamorphic (HT–UHPM) rocks in the geological record (e.g. Yamato *et al.*, 2008; Li & Gerya, 2009 and references therein). An exception is the model developed by Li & Gerya (2009), in which the formation and exhumation of HT–UHPM rocks is achieved. This model predicts the development of a sub-lithospheric plume of crustal material that undergoes strong conductive heating from the surrounding hot asthenosphere of the mantle wedge during a prolonged residence of 10–20 Ma at HT–UHPM conditions before upward extrusion of the melt-bearing materials transports them toward the surface (Li & Gerya, 2009, Fig. 8).

The elevated peak temperatures of some UHPM rocks suggest the possibility of their melting at UHPM conditions, although at these pressures a distinction between K-, Na- and Si-rich fluids and hydrous silicate melts is impossible, because the system is in the supercritical state (Stoeckhert *et al.*, 2001). Based on examples of exposed UHPM rocks, which commonly exhibit leucosome at outcrop and may contain polymineralic inclusions after melt or supercritical fluid in refractory minerals such as garnet (e.g. Andersen & Osmundsen, 1994; Zhong *et al.*, 2001; Labrousse *et al.*, 2002; Wallis *et al.*, 2005; Lang & Gilotti, 2007; Ragozin *et al.*, 2009; Zeng *et al.*, 2009; Gao *et al.*, 2012), melting generally has occurred around the metamorphic peak or during exhumation in many UHPM terranes. This could be extremely important in the evolution and exhumation of these UHPM rocks, for example by increasing buoyancy and

decreasing strength. Some of the numerical models discussed above show that partial melting of deeply subducted continental crust and associated sedimentary rocks could occur, consistent with both field geology (references above) and petrological phase relations (Hermann & Green, 2001; Skjerlie & Patino Douce, 2002; Auzanneau *et al.*, 2006; Massonne, 2009), leading to the suggestion that the presence of melt could be a contributing factor in the exhumation of these UHPM rocks (e.g. Gerya *et al.*, 2008; Li & Gerya, 2009; Vrijmoed *et al.*, 2009).

In this study a series of 2D petrological–thermo-mechanical numerical experiments was undertaken to: (i) characterize the variability of exhumation mechanisms of UHPM rocks during collision of spontaneously moving plates and (ii) investigate the possible geodynamic effects of melting at ultrahigh pressure conditions for the exhumation of HT–UHPM rocks. The results of this study demonstrate that the model UHPM complexes indeed develop high temperature conditions above the solidus (melt-present) at ultrahigh pressures and that exhumation of these model UHPM complexes does produce realistic upper-crustal structures. Sensitivity studies performed during the series of experiments reported here suggest that some previously proposed mechanisms for the exhumation of UHPM rocks are also accessed within the parameter space investigated.

## NUMERICAL MODEL DESIGN

The 2D petrological–thermomechanical numerical model used in this work simulates the processes of oceanic plate subduction followed by continental collision in a 4000 km × 1400 km lithosphere/asthenosphere section. The model is based on the I2VIS code (Gerya & Yuen, 2003a) using conservative finite differences and a non-diffusive marker-in-cell technique to simulate multiphase flow. In the first model (model I), which is used as a reference frame as the main parameters are varied in models II to V, a 40 Ma old oceanic plate with a width of 400 km is located between two continental plates, but forming part of the left-hand composite oceanic/continental plate (Fig. 1). The right-hand continental plate is 1700 km wide and fixed whereas the left-hand continental plate is 1860 km wide and is initially pushed to the right with a constant velocity of 5 cm year<sup>-1</sup> imposed in a small domain in the continental lithosphere at the left edge of the model. The push is maintained for the first 6–8 Ma of model evolution until the left-hand continent reaches the right-hand continent after which the push is discontinued and subduction is driven spontaneously by slab pull. Thus, the collision stage in the model evolves self-consistently according to a spontaneous plate convergence velocity regulated by the slab pull, asthenospheric viscosity and buoyancy of the subducting continental crust. The models use a grid resolution of 1361 × 351 nodes with variable grid spacing.

This allows a minimum grid resolution of 1 km in the area of interest covering 1050 km horizontally (from  $x = 1900$  to 2950 km) and 250 km vertically (from  $z = 0$  to 250 km). The number of lagrangian markers is ~13 million.

In model I, on the left the oceanic lithosphere is attached abruptly to the continental lithosphere with sedimentary rocks overlying a narrow passive margin (50 km wide), whereas on the right a prism of sedimentary rocks is set against the continent above a weak zone along the left edge of the right-hand continental plate (Fig. 1). The cooling age of the oceanic lithosphere is 40 Ma. The oceanic crust is represented by 2 km of hydrothermally altered basalts underlain by 5 km of gabbroic rocks. The upper continental crust is felsic (thickness is 20 km with a weaker rheology of wet quartzite, Table 1) whereas the lower continental crust is mafic (thickness is 20 km with a stronger rheology of plagioclase An<sub>75</sub>, Table 1). At the onset of subduction, both the lithospheric mantle and the asthenosphere consist of anhydrous peridotite. During the process of subduction, the mantle overlying the subducting slab becomes hydrated as a result of migration of fluid liberated by metamorphic reactions in the slab. The stable fluid content for each lithology was obtained by using free energy minimization (Connolly, 2005). The flow law for each lithology and other physical parameters for the experiments are presented in Table 1.

Subduction of the oceanic plate is initiated by prescribing a weak zone in the mantle with the rheology of wet olivine (Ranalli, 1995) and low plastic strength (internal friction coefficient of 0.1) between the oceanic lithospheric mantle and the right-hand subcontinental lithospheric mantle (e.g. Toth & Gurnis, 1998). The weak zone extends from the bottom of the continental crust to the bottom of the subcontinental lithospheric mantle (140 km). The chemical density contrast between the subcontinental lithospheric mantle and the underlying asthenospheric mantle is 20 kg m<sup>-3</sup> (Djoman *et al.*, 2001).

All mechanical boundary conditions are free-slip (cf. Gorczyk *et al.*, 2007), and the left-hand continental plate is initially decoupled from the left boundary of the model by a vertical 20 × 150 km zone of lowered viscosity (10<sup>20</sup> Pa s). The top surface of the lithosphere is treated as an internal free surface by using a 20–22 km thick top layer with low viscosity (10<sup>18</sup> Pa s) and density (1 kg m<sup>-3</sup> for air and 1000 kg m<sup>-3</sup> for sea water below  $z = 20$  km level). The large viscosity contrast caused by these low viscosity boundary layers minimizes shear stresses (<10<sup>4</sup> Pa) at the top of the lithosphere making it an efficient free surface (cf. Schmeling *et al.*, 2008). This upper boundary evolves by erosion and sedimentation according to the following Eulerian transport equation (Gerya & Yuen, 2003a; Gorczyk *et al.*, 2007),

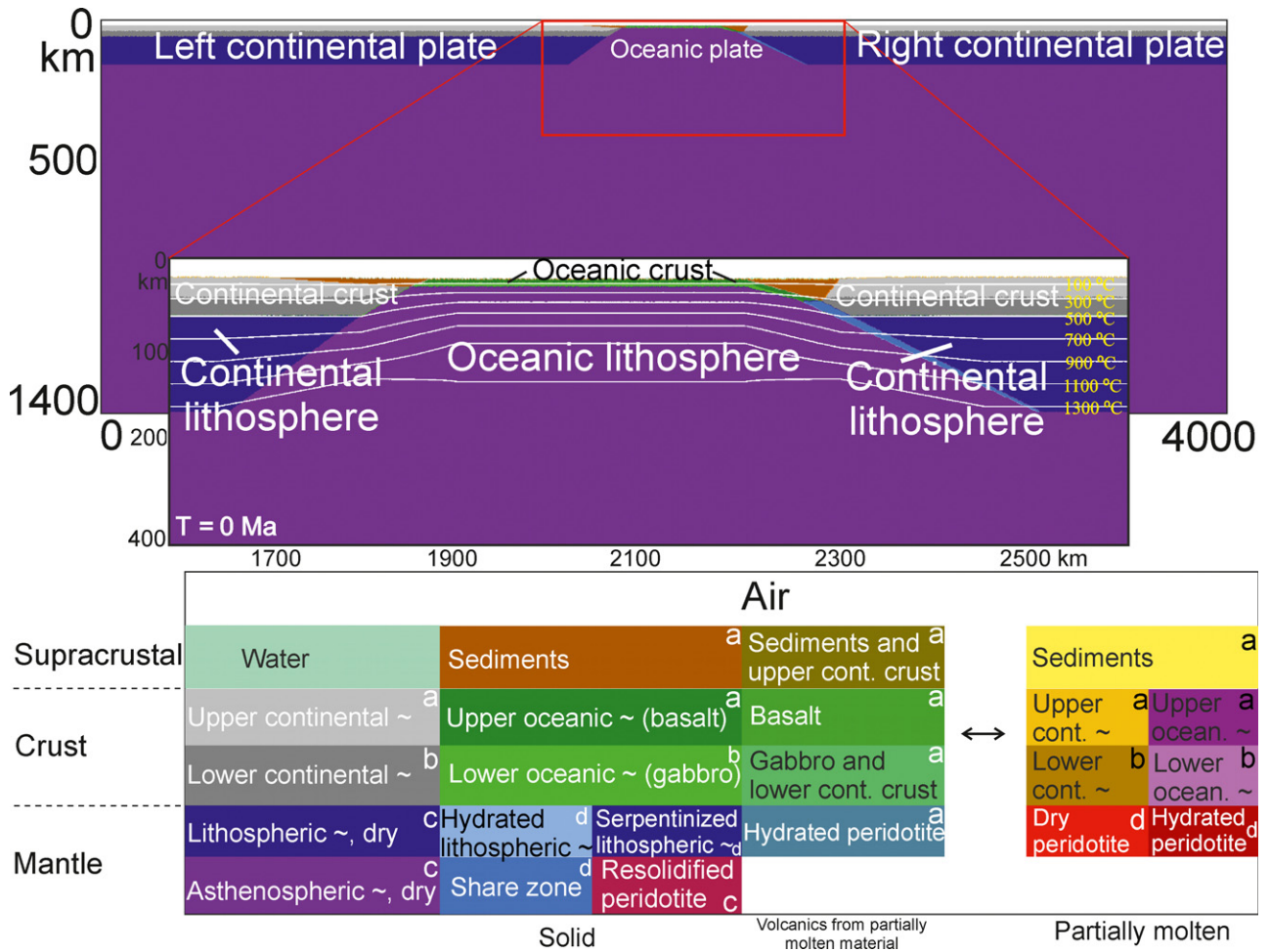


**Fig. 1.** Initial configuration of the numerical model [see text, Supporting Information and Sizova *et al.* (2010) for details]. White lines are isotherms shown for increments of 200 °C starting from 100 °C. Colours indicate materials (e.g. rock type or melt-bearing rock type) that appear in subsequent figures. Letters a, b, c, d show the rheology that is used for each of the materials (see Table 1): a – wet quartzite; b – plagioclase An75; c – dry olivine; d – wet olivine. The resolution of the model at  $x = 1900\text{--}2950$  km and  $y = 0\text{--}250$  km is  $1 \times 1$  km, but in the remaining part of the model the resolution gradually changes to up to  $10 \times 10$  km.

$$\frac{\partial z_{es}}{\partial t} = v_z - v_x \frac{\partial z_{es}}{\partial x} - v_s + v_e, \quad (1)$$

where  $z_{es}$  is the vertical position of the surface as a function of the horizontal distance  $x$ ,  $v_z$  and  $v_x$  are the vertical and horizontal components of the material velocity vector at the surface, and  $v_s$  and  $v_e$  are the sedimentation and erosion rates, respectively. The sedimentation and erosion rates correspond to the following relations,

$$v_s = 0 \text{ mm year}^{-1}, \quad v_e = v_{e0} \text{ mm year}^{-1}, \quad \text{when } z < z_{sea}, \text{ and}$$

$$v_s = v_{s0} \text{ mm year}^{-1}, \quad v_e = 0 \text{ mm year}^{-1}, \quad \text{when } z > z_{sea},$$

where  $v_{e0} = 0.03 \text{ mm year}^{-1}$  and  $v_{s0} = 0.03 \text{ mm year}^{-1}$  are the imposed erosion and sedimentation rates, respectively, and  $z_{sea} = 20$  km is the sea-level prescribed in the model.

The initial temperature field for the oceanic lithosphere is derived from the oceanic geotherm computed for the given cooling age and the temperature of the asthenospheric upper mantle (Turcotte & Schubert, 2002). In the continental lithosphere, the initial thermal structure is determined based on the radiogenic heat production of the upper and the lower crust, where the surface temperature (0 °C) and the upper-mantle temperature at the bottom of the lithosphere (1344 °C at 140 km) are prescribed. The initial temperature gradient in the underlying mantle is  $0.5 \text{ °C km}^{-1}$ . During the numerical experiments this initial thermal structure evolves spontaneously.

Because the  $\text{H}_2\text{O}$  transport model does not permit complete hydration of the peridotitic mantle, the mantle solidus is intermediate between the wet and dry peridotite solidi. In reality, variable hydration would permit melting over a range of temperatures and water contents (e.g. Grove *et al.*, 2006). To account for this

**Table 1.** Properties of the materials used in the experiments (Bittner & Schmelting, 1995; Clauser & Huenges, 1995; Ranalli, 1995; Schmidt & Poli, 1998; Turcotte & Schubert, 2002; Burg & Gerya, 2005).

Material <sup>a</sup>	$\rho_0$ [kg m <sup>-3</sup> ] (solid)	$k$ [W (m <sup>2</sup> K) <sup>-1</sup> ]	Rheology/ flow law	$T_{\text{solidus}}$ [K]	$T_{\text{liquidus}}$ [K]	$H_r$ [ $\mu$ W m <sup>-2</sup> ]	$H_L$ [kJ kg <sup>-1</sup> ]	$E$ [kJ mol <sup>-1</sup> ]	$n$	$A_D$ [MPa <sup>-1</sup> s <sup>-1</sup> ]	$V$ [J (MPa *mol) <sup>-1</sup> ]	Cohesion [MPa]	sin ( $\phi$ dry)
Sedimentary and felsic crust	Sediments:2600 Felsic crust: 2700	$0.64 + \frac{807}{(T+77)}$ $\times \exp(0.00004 \cdot P_{M/P_0})$	Wet quartzite	at $P < 1$ $889 + \frac{17900}{(P+54)} + \frac{20200}{(P+54)^2}$ at $P > 1200$ Mpa $831 + 0.06 \cdot P$	$1262 + 0.009 \cdot P$	2 Felsic crust:1	300	154	2.3	$10^{-3.5}$	0	10	0.15
Melt-bearing sediments and felsic crust	2400	-/-	-/-***	-/-	-/-	-/-	-/-	0	1	-/-	-/-	1	0
Basalts	3000	$[1.18 + \frac{474}{(T+77)}]$ $\times \exp(0.00004 \cdot P_{M/P_0})$	Wet quartzite	at $P < 1600$ MPa $973 - \frac{70400}{(P+354)} + \frac{27800000}{(P+354)^2}$ at $P > 1600$ MPa $935 + 0.0035 \cdot P + 0.0000062 \cdot P^2$	$1423 + 0.105 \cdot P$	0.25	380	154	2.3	$10^{-3.5}$	0	10	0.1
Melt-bearing basalts	2900	-/-	-/-	-/-	-/-	-/-	-/-	0	1	-/-	-/-	1	0
Gabbroic/mafic crust	3000	$[1.18 + \frac{474}{(T+77)}]$ $\times \exp(0.00004 \cdot P_{M/P_0})$	Plagioclase Ab <sub>75</sub>	-/-	$1423 + 0.105 \cdot P$	0.25	380	238	3.2	$10^{-3.5}$	0	10	0.6
Melt-bearing gabbroic/mafic crust	2900	-/-	Wet quartzite	-/-	-/-	-/-	-/-	0	1	-/-	-/-	1	0
Lithosphere-asthenosphere mantle	3300	$[0.73 + \frac{1293}{(T+77)}]$ $\times \exp(0.00004 \cdot P_{M/P_0})$	Dry olivine	$1394 + 0.133 \cdot P_{M/P_0}$ $-0.0000051 \cdot P_{M/P_0}^2$	$2073 + 0.114 \cdot P$	0.022	-	532	3.5	$10^{4.4}$	8	10	0.6
Hydrated mantle/hydrated mantle in subduction zone/serpentinized mantle	3200 (hydrated) 3000 (serpentinized) 3300 (shear zone)	-/-	Wet olivine	Hydrated mantle: at $P < 1600$ Mpa: $973 + \frac{70400}{(P+354)} + \frac{27800000}{(P+354)^2}$ at $P > 1600$ Mpa: $935 + 0.0035 \cdot P + 0.0000062 \cdot P^2$	Hydrated mantle: 2073 + 0.114 · P	0.022	Hydrated mantle: 300	470	4	$10^{3.3}$	-/-	10	0.1
Dry/wet melt-bearing mantle	3300/2900	-/-	Dry/wet olivine	-/-	-/-	-/-	-	0	1	$10^{4.4}$	-/-	1	0
Reference <sup>b</sup>	1,2	3	4	5	5	1	1,2	4	4	4	4	4	4,1

$\rho_0$ , density;  $k$ , thermal conductivity;  $T_{\text{solidus,liquidus}}$ , solidus and liquidus temperatures of the crust;  $H_r$ ,  $H_L$ , heat production (radiogenic, latent);  $E$ , activation energy;  $n$ , stress component;  $A_D$ , material constant;  $V$ , activation volume; sin( $\phi$ dry), effective friction coefficient for dry rocks.  
<sup>a</sup>For all types of rocks:  $C_0 = 1000$  J kg<sup>-1</sup>,  $\alpha = 3 \cdot 10^{-5}$  K<sup>-1</sup>,  $\beta = 1 \cdot 10^{-3}$  MPa<sup>-1</sup>.  
<sup>b</sup>1 = (Turcotte & Schubert, 2002), 2 = (Bittner & Schmelting, 1995), 3 = (Clauser & Huenges, 1995), 4 = (Ranalli, 1995), 5 = (Schmidt & Poli, 1998).  
 \*\*\* The same property as for the previous material.

behaviour we assume that the degree of both hydrous and dry melting is a linear function of pressure and temperature (e.g. Gerya & Yuen, 2003b). In this model, the volumetric degree of melting  $M_0$  is,

$$M_0 = \begin{cases} 0 & T < T_{\text{solidus}} \\ \frac{T - T_{\text{solidus}}}{T_{\text{liquidus}} - T_{\text{solidus}}} & T_{\text{solidus}} < T < T_{\text{liquidus}}, \\ 1 & T > T_{\text{liquidus}} \end{cases} \quad (2)$$

where  $T_{\text{solidus}}$  and  $T_{\text{liquidus}}$  are, respectively, the solidus temperature (wet and dry solidi are used for the hydrated and dry mantle, respectively) and the dry liquidus temperature at a given pressure and rock composition (see Table 1). To simulate melt extraction from partially molten rocks (e.g. Nikolaeva *et al.*, 2008; Gerya & Meilick, 2011) we define a melt extraction threshold  $M_{\text{max}}$  and a non-extractable amount of melt  $M_{\text{min}} < M_{\text{max}}$  that will remain in the source. The influence of these parameters on subduction dynamics and crustal growth is investigated for the case of constant  $M_{\text{max}}/M_{\text{min}} = 2$ .

Markers track the amount of melt extracted during the evolution of each experiment. The total amount of melt,  $M$ , for every marker takes into account the amount of previously extracted melt and is calculated as,

$$M = M_0 - \sum_n M_{\text{ext}} \quad (3)$$

where  $\sum_n M_{\text{ext}}$  is the total melt fraction extracted during the  $n$  previous  $n$  extraction episodes. Once the total amount of melt,  $M$ , computed from equations (2) and (3) for a given marker exceeds  $M_{\text{max}}$ , the extractable melt fraction  $M_{\text{ext}} = M - M_{\text{min}}$  is assumed to migrate upward and the value of  $\sum_n M_{\text{ext}}$  is updated. We assume that melt migration is rapid compared with the deformation of unmelted mantle, so that the velocity of the melt is independent of mantle dynamics (Elliott *et al.*, 1997; Hawkesworth *et al.*, 1997). Thus, the extracted melt is transported instantaneously to the surface forming new volcanic crust above the extraction area.

The weakening effects of ascending fluids and melts are included into the model (Sizova *et al.*, 2010; Gerya & Meilick, 2011). During aqueous fluid propagation from the slab the yield strength,  $\sigma_{\text{yield}}$ , of the percolated rocks is decreased according to  $\lambda_{\text{fluid}} = 1 - P_{\text{fluid}}/P_{\text{solid}}$  (see Appendix S1 for details). Similarly, during a melt extraction episode, the yield strength,  $\sigma_{\text{yield}}$ , of rock in the column between the source of the melt and the surface is decreased according to  $\lambda_{\text{melt}} = 1 - P_{\text{melt}}/P_{\text{solid}}$ . A low value of  $\lambda_{\text{fluid}} = \lambda_{\text{melt}} = 0.001$  was used in the numerical experiments providing significant weakening of rocks subjected to free fluid/melt propagation and creating favourable conditions for realistic modern-style subduction (Sizova *et al.*, 2010).

The compressibility of the subducting oceanic crust was increased by a factor of two relative to other rocks. This allowed simulation to a first order of the

effects of an increased slab pull related to the eclogitization reaction in the subducting slab (e.g. Mishin *et al.*, 2008; Baumann *et al.*, 2010). A more detailed description of the model and the numerical techniques employed in this study are given in Appendix S1.

## EXPERIMENTAL RESULTS

For this investigation of mechanisms of exhumation of UHPM rocks a range of experiments involving continental collision of spontaneously moving plates, subduction of the continental lithosphere and oceanic slab detachment was undertaken. Based on changes in several parameters in the models – the length of the oceanic lithosphere component of the left hand plate (300, 400, 500 and 600 km), which is responsible for the strength of the slab pull, and the width of the passive margin [either abrupt (50 km) or gradual (150 km)], which affects the subductability of the continental lithosphere, where these two parameters represent the main axes of the sensitivity study illustrated in Fig. 2, and the presence of melting – five distinct (U)HPM exhumation modes associated with different major collision scenarios were identified: vertical crustal extrusion, large-scale crustal stacking, shallow crustal delamination, trans-lithospheric diapirism and channel flow.

### Numerical experiments with melting

*Model 1: 400 km long oceanic plate with an abrupt passive margin*

Figures 3–5 represent the evolution of model I, which results in the formation and exhumation of HT–UHPM crustal rocks with very high peak metamorphic temperatures (up to 1000 °C, Fig. 4c') that are 100–400 °C higher than maximal peak temperatures achieved in experiments with a prescribed plate convergence velocity (e.g. Burov *et al.*, 2001; Gerya *et al.*, 2008; Warren *et al.*, 2008a,b; Li & Gerya, 2009). During the early evolution of the model, the oceanic lithosphere is subducted and the ocean basin closes (Figs 3a & 4a). When the subducting oceanic lithosphere reaches 100 km depth the oceanic crust starts to dehydrate and partially melt, which leads to hydration of the overlying mantle and wet melting above the slab (Figs 3a & 4a). In accordance with the high degree of melt and fluid weakening adopted ( $\lambda_{\text{fluid}} = \lambda_{\text{melt}} = 0.001$ ), the overriding lithosphere is extended and a back-arc basin with ~3 km of volcanic rocks is developed.

At the beginning of the continental collision stage, after the ocean basin has closed completely, the incoming continental margin starts to subduct. By this stage, the initially imposed push of the left-hand continental plate to the right has been deactivated and continental subduction is driven spontaneously by slab

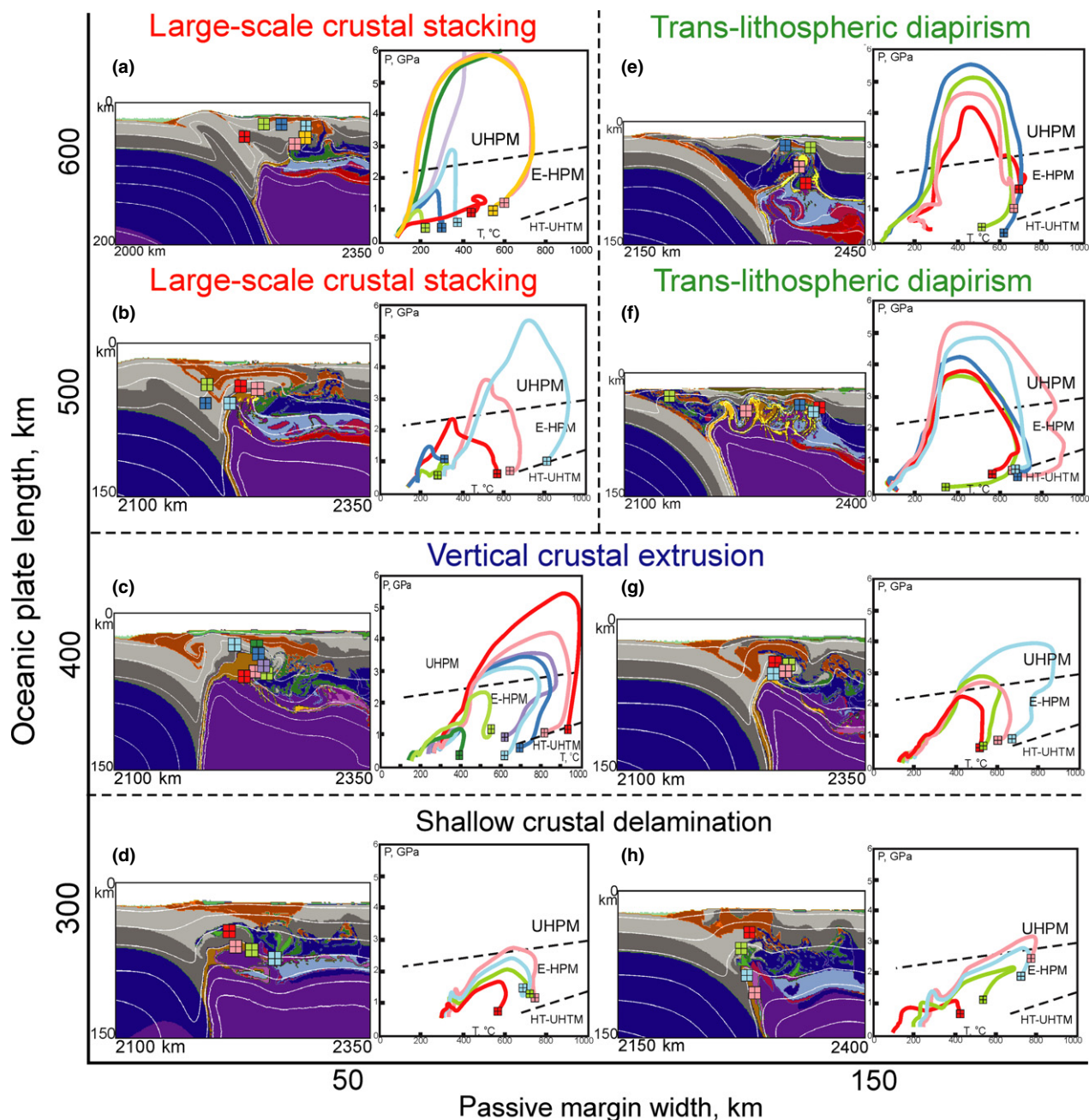


**Fig. 2.** Schematic representation of the results of the sensitivity study of collision styles and exhumation mechanisms for (U)HPM rocks. The study involved varying the length of the oceanic plate (from 300 to 600 km) and the width of the passive margin (a prescribed space for the thinning of the continental crust towards the oceanic plate, either 50 or 150 km). For each experiment a representative snapshot from the model evolution and the  $P$ - $T$ - $t$  paths recorded are shown. Corresponding models are shown in the following figures: (a) = Fig. 7, (b) = Fig. 9, (c) = Fig. 4, (d) = Fig. 10, (e) = Fig. 13, (f) = Fig. 14, (g) = Fig. 15, and (h) = Fig. 11. See text for discussion.

pull. As the spontaneous collision process evolves the topographic elevation increases (see the topography profiles on Figs 4b & 5a,a') and the dip of the slab steepens to vertical (Figs 3b & 4b). After the subducting continental lithosphere reaches a depth of 60 km most of the upper continental crust starts to

delaminate from the lower continental crust and accretes to the overriding plate within the subduction channel (Fig. 4b). The lower rheologically stronger continental crust continues to be subducted, together with a thin remnant (~3 km thick) of the upper continental crust.

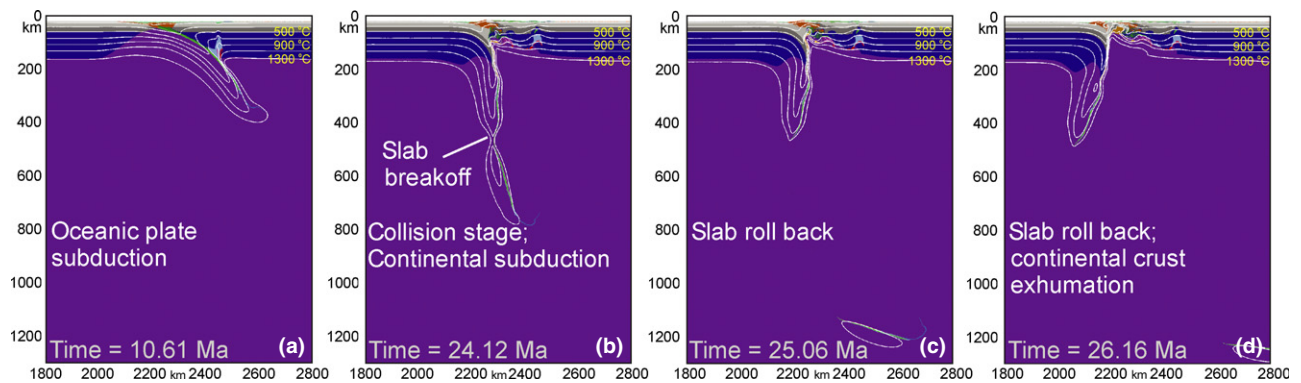


**Fig. 3.** Four time-slice snapshots to show the large-scale evolution of model I (vertical crustal extrusion), which has a 400 km long oceanic plate and an abrupt passive margin (50 km wide), up to slab roll back and exhumation of the subducted continental crust. 1000 × 1300 km sections of the original 4000 × 1400 km model are shown. Colour code is the same as in Fig. 1. Detailed development of the collision zone for this model is shown in Fig. 4.

The positive buoyancy of the subducted continental crust causes a gradual decrease in the subduction velocity that in turn triggers thermal relaxation of the subducted lithosphere. After the collision stage was initiated (*c.* 12 Ma), the subduction is terminated by slab breakoff, which does not localize at the oceanic lithosphere–continental lithosphere transition but occurs at a much greater depth of ~400 km in the oceanic part of the slab (Fig. 3b). Slab detachment in the form of a viscous dripping instability in this model (see Fig. 3b) is commonly characteristic of relatively warm subducted slab segments with a core temperature above 1000 °C (Gerya *et al.*, 2004a; Duretz *et al.*, 2011). In model I, this elevated slab temperature forms in response to slow subduction caused by the limited slab pull of the relatively short oceanic plate prescribed in this experiment. As the subduction velocity decreases, the short subducted slab is hanging in the mantle undergoing heating by conduction from the surrounding asthenosphere, until detachment of the hottest and deepest segment of the slab is triggered (Fig. 3b).

After detachment, the weight of the remaining portion of the hanging slab is not sufficient to overcome the positive buoyancy of the continental crust, which ceases to subduct at ~200 km depth. The system remains essentially static for *c.* 0.5 Ma and the deep detachment event does not exert any instantaneous influence on the system. A small component of slab rollback and extension of the overriding plate resume after the 0.5 Ma hiatus (Figs 3c & 5b,b') leading to ascent of hot asthenosphere (compare Fig. 5a' with Fig. 5b'). In turn, this leads to smoothing of the high topography developed during the initial collision stage as the orogen widens (Fig. 4c,d).

During the period of slow continental subduction the continental crust is subjected to heating as the continental side of the vertically hanging slab comes into contact with the hot asthenospheric mantle of the wedge for a prolonged period of time (*c.* 2 Ma), which

allows conductive heating and partial melting of the remnant of upper continental crust and the lower continental crust at ultrahigh pressures. As a result, the positive buoyancy of the continental crust is enhanced and the overlying material becomes strongly weakened by percolating UHP melts (according to the high degree of melt weakening adopted, where  $\lambda_{\text{melt}} = 0.001$ ). This facilitates exhumation of the buoyant melt-bearing UHP crustal rocks vertically towards the surface along the slab–mantle interface (Figs 3c,d, 4c,d & 5a,a',b,b'). The melt-bearing continental crust moves upward along the slab–mantle interface in the form of a gently curved planar (wave-like) structure (see yellow-coloured layer in Fig. 5b, and the ascent channel in Fig. 5b'). Similar buoyant wave-like structures forming against slabs have been previously described in 2D and 3D numerical experiments of oceanic plate subduction (Gerya *et al.*, 2004b; Zhu *et al.*, 2009). The partially molten UHP crust is exhumed to depths of 10–40 km forming a plume-like body ~50 km across in the lower crust of the extending collision zone (Fig. 4d).

The metamorphic *P–T* conditions for the subducted continental crust through time were traced using markers (lagrangian particles; Fig. 4, *P–T–t* paths). All markers were initially placed inside the left-hand continental plate margin, with three markers (dark green, green and violet) in the upper continental crust and four markers (blue, light blue, pink and red) in the lower continental crust. During the process of subduction all markers show increasing pressure and temperature (Fig. 4a'). Whereas the initial spacing of the markers was limited (< 40 km horizontal distance between markers), at the time of the slab breakoff they show a large variation in depth (up to 150 km) and in *P–T* conditions (from 1 GPa at 400 °C up to 5.5 GPa at 900 °C), with peak *P–T* for five of the seven markers corresponding to HT-UHPM conditions (Fig. 4b'). The decompression segments of the *P–T–t* paths are different, with crustal material subducted no deeper

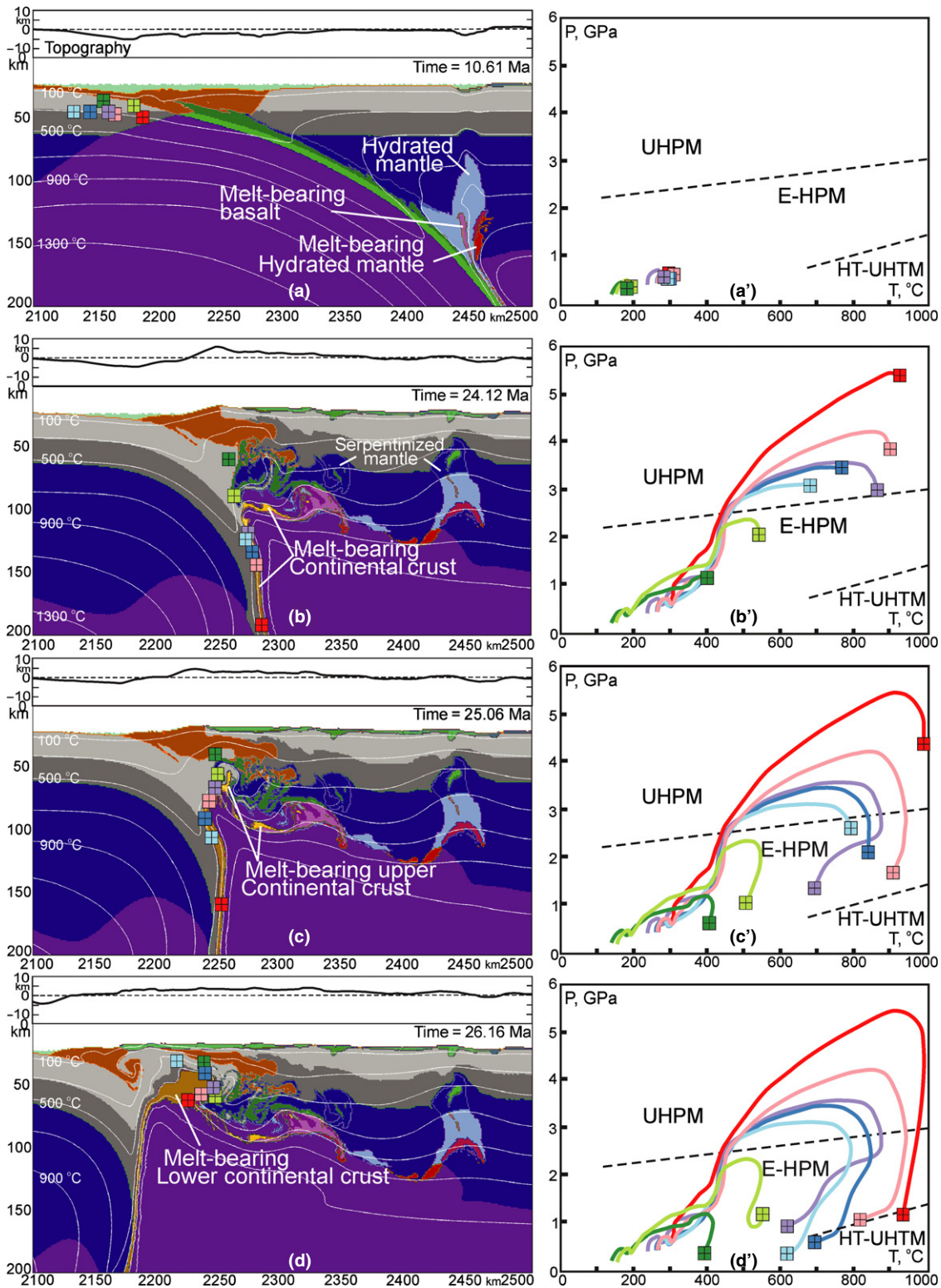


**Fig. 4.** Four time-slice snapshots to show the development of the continental collision zone in model I (left column) and the associated representative  $P$ - $T$ - $t$  paths for crustal rocks (right column).  $400 \times 200$  km sections of the original  $4000 \times 1400$  km model are shown. The topographic profile for each snapshot is given on the top. Coloured squares on the snapshots are markers that refer to the diagrams with the  $P$ - $T$ - $t$  paths (a'-d'). The dashed lines separate fields for different types of metamorphism (Brown, 2007): UHPM = ultrahigh pressure metamorphism; E-HPM = eclogite-high pressure granulite metamorphism; UHTM = ultrahigh pressure metamorphism. Colour code is the same as in Fig. 1.

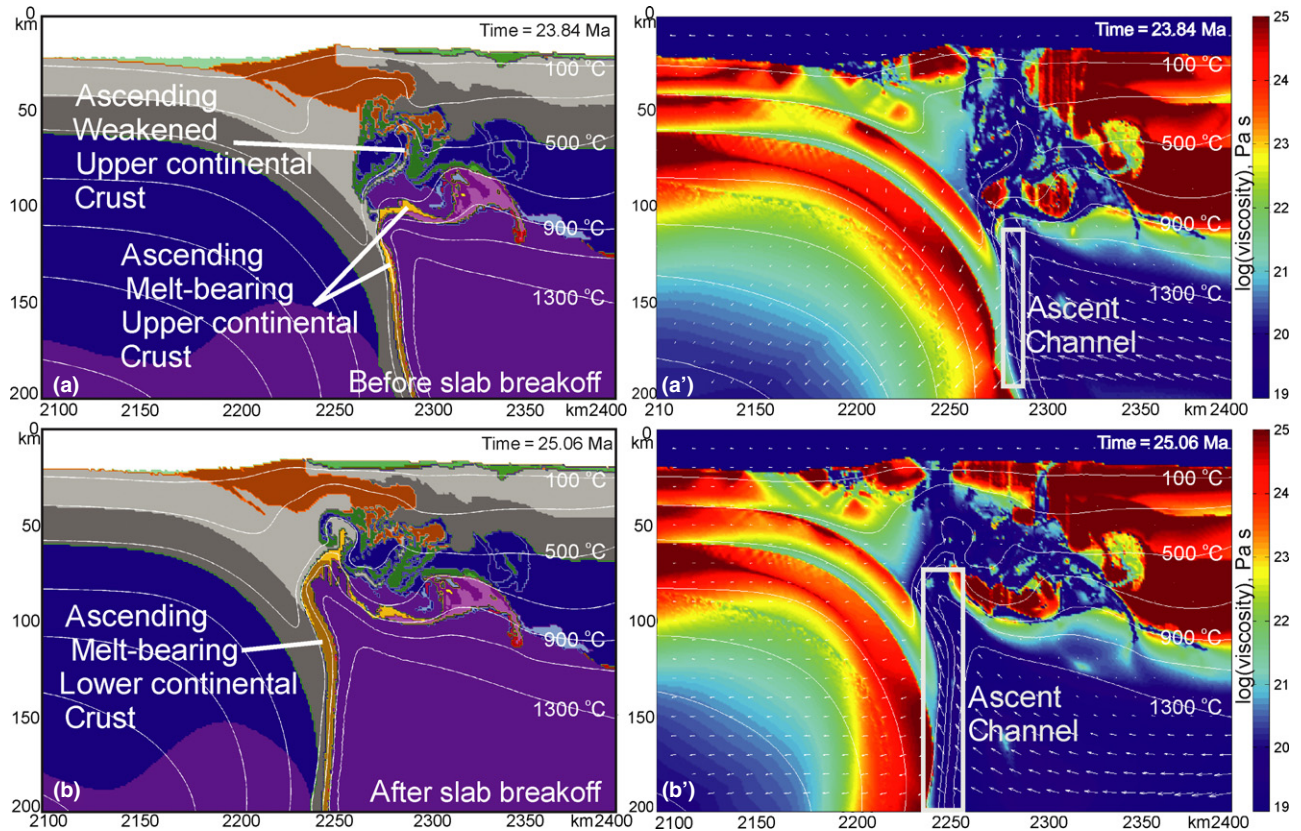


**Fig. 5.** Vertical ascent (extrusion) of partially molten UHPM crustal rocks along the slab in model I. Representative  $300 \times 200$  km snapshots (left column) are shown with the respective effective viscosity fields (right column). Colour code in the left column is the same as in Fig. 1. White arrows in the snapshots in the right column show the calculated velocity field, colours represent the magnitude of effective viscosity (see the colour bar), and rectangles outline an area of crustal ascent (extrusion) along the slab–mantle wedge interface. The vertical low viscosity ascent channel in the mantle wedge and the overriding plate is formed due to the imposed rheological weakening by ascending melts ( $\lambda_{\text{melt}} = 0.001$ ) formed in the subduction channel under the overriding plate (see yellow and pink areas in the snapshots in the left column). Snapshots a and a' represent the buoyant ascent of the melt-bearing upper continental crust before slab breakoff. Snapshots b and b' show the melt-bearing lower continental crust moving vertically upward along the slab–mantle interface in the form of a gently curved planar (wave-like) structure after slab breakoff.

than 120 km being exhumed to middle crustal depths along tighter  $P$ – $T$ – $t$  loops (Fig. 4c',d' violet, blue markers), whereas the more deeply subducted crustal material, which always underlies the early exhumed materials at middle crustal depths, has more open  $P$ – $T$ – $t$  loops with a larger segment of near-isothermal decompression close to peak temperature (Fig. 4c',d' red and pink markers).

Parts of the upper continental crust that remained at temperatures below the solidus also become involved in the exhumation process and represent rocks that occur above and below the UHPM rocks in nature. These areas are characterized by high pressure (Fig. 4c',d' dark green and green markers) or lower-grade metamorphism.

*Model II: 600 km long oceanic plate with an abrupt passive margin*

Figures 6–8 represent the evolution of an experiment in which the length of the oceanic lithosphere

component of the left hand plate is increased by 50% to 600 km (compared with 400 km in the previous model). Subduction of this longer segment of oceanic lithosphere produces an increased length of slab and consequently a stronger slab pull, faster convergence velocity and more rapid slab detachment (compare Fig. 3b with Fig. 6c) during the spontaneous collision phase.

The internal evolution and geometry of the continental collision zone is very different from the previous model. As the ocean basin closes at *c.* 10–11 Ma (Figs 6a & 7a) the incoming continental passive margin begins to subduct in a coherent manner reaching depths of 100–150 km within 6 Ma after the initiation of collision (Fig. 7b). Buoyancy of the deeply subducted continental crust creates large deviatoric stresses, which trigger brittle/plastic failure along the subducted Moho boundary (Fig. 7b). A large coherent crustal-scale block of continental crust separates from the subducting plate and is thrust back over the subducting plate along a major shear zone producing

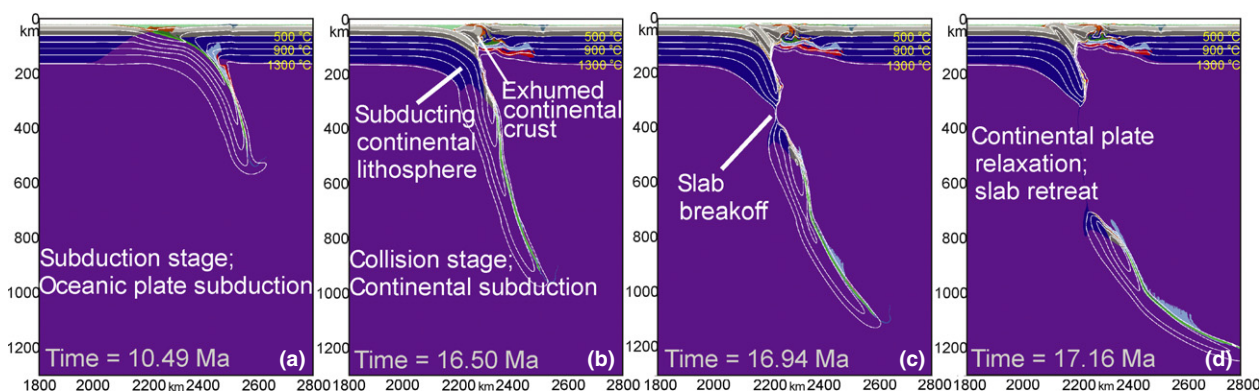


**Fig. 6.** Four time-slice snapshots to show the large-scale evolution of model II (large-scale crustal stacking), which has a 600 km long oceanic plate and an abrupt passive margin (50 km wide), up to continental plate relaxation and slab retreat.  $1000 \times 1300$  km sections of the original  $4000 \times 1400$  km model are shown. Colour code is the same as in Fig. 1. Detailed development of the collision zone for this model is shown in Fig. 7.

extremely rapid exhumation of UHP rocks within 0.2–0.3 Ma (Figs 6b, 7c & 8a,a'). Strong shear heating inside the shear zone results in localized melting of the continental crust (Fig. 8a). As the continental lithosphere continues to subduct, a second large-scale crustal stacking event takes place *c.* 0.5 Ma after the first (Figs 7d & 8b,b').

During ascent of the second block of continental crust subduction is terminated by slab breakoff, which localizes in the continental part of the subducting plate at a depth of 300 km (Figs 6c,d & 7d). The breakoff exerts an instantaneous influence on the system resulting in a period of relaxation of the overriding continental plate, which causes a further increase of the elevation of the orogen. After 2000 years slab rollback resumes and drives extension of the orogeny (see the topography profiles on Fig. 7a–d).

The subducted continental crust and associated sedimentary rocks rapidly reach a depth of 140 km and then return to mid-to-lower crustal depths in less than 1 Ma. Overall, there is insufficient time for conductive heating from the hot asthenosphere of the mantle wedge to raise temperatures as high as in model I. As a result, partial melting is localized rather than widespread and melt-induced buoyancy does not contribute to the exhumation of the UHP rocks. The metamorphic  $P$ – $T$  conditions for the subducted continental crust and associated sedimentary rocks through time were traced using markers (lagrangian particles; Fig. 7 a'–d'). All markers were initially placed in the left-hand continental margin, with two markers (yellow and pink) in the sedimentary rocks and six markers (lilac, dark green, green, blue, dark blue and red) in the upper continental crust (Fig. 7a). The marker locations in the sedimentary rocks spend longer in contact with the hot asthenospheric mantle of the wedge than those in the continental crust and consequently they define open  $P$ – $T$ – $t$  loops with maximum temperatures of  $\sim 750$  °C at UHPM con-

ditions (Fig. 7a'–d'). In contrast, the marker locations in the upper continental crust (i.e., in the interior of the coherently moving crustal block) define very tight  $P$ – $T$ – $t$  loops, in some cases reaching UHPM conditions but at extremely low temperatures ( $< 400$  °C; Fig. 7a'–d') because of the very rapid continental subduction and exhumation associated with the large-scale crustal stacking.

An experiment with an intermediate oceanic plate length of 500 km shows a transitional type of evolution between the models I and II (compare Fig. 9 with Figs 4 & 7). Slab breakoff occurs at the oceanic lithosphere–continental lithosphere transition and coincides with limited stacking of the deeply subducted continental crust, similar to the experiment with the longest oceanic plate (compare Fig. 9c with Fig. 7b). Afterwards, the most deeply subducted lower continental crust is exposed to conductive heating from the surrounding hot asthenosphere of the mantle wedge at UHPM conditions, undergoes partial melting and is exhumed towards the surface (Fig. 9a'–d' light blue and pink markers). Less deeply subducted continental crust does not reach UHPM conditions (Fig. 9a'–d' red, blue and green markers). This mode of exhumation (vertical crustal extrusion) of the most deeply subducted (melt-bearing) lower continental crust is similar to the exhumation mechanism in model I and as in model I the UHPM rocks record high-temperature conditions at ultrahigh pressures (compare Fig. 9d with Fig. 4c,d).

#### *Model III: 300 km long oceanic plate with an abrupt passive margin*

Figure 10 represents the evolution of an experiment in which the length of the oceanic lithosphere component of the left hand plate is decreased by 25% to 300 km (compared with 400 km in model I), but still with an abrupt passive margin (Fig. 10a). Subduction of this

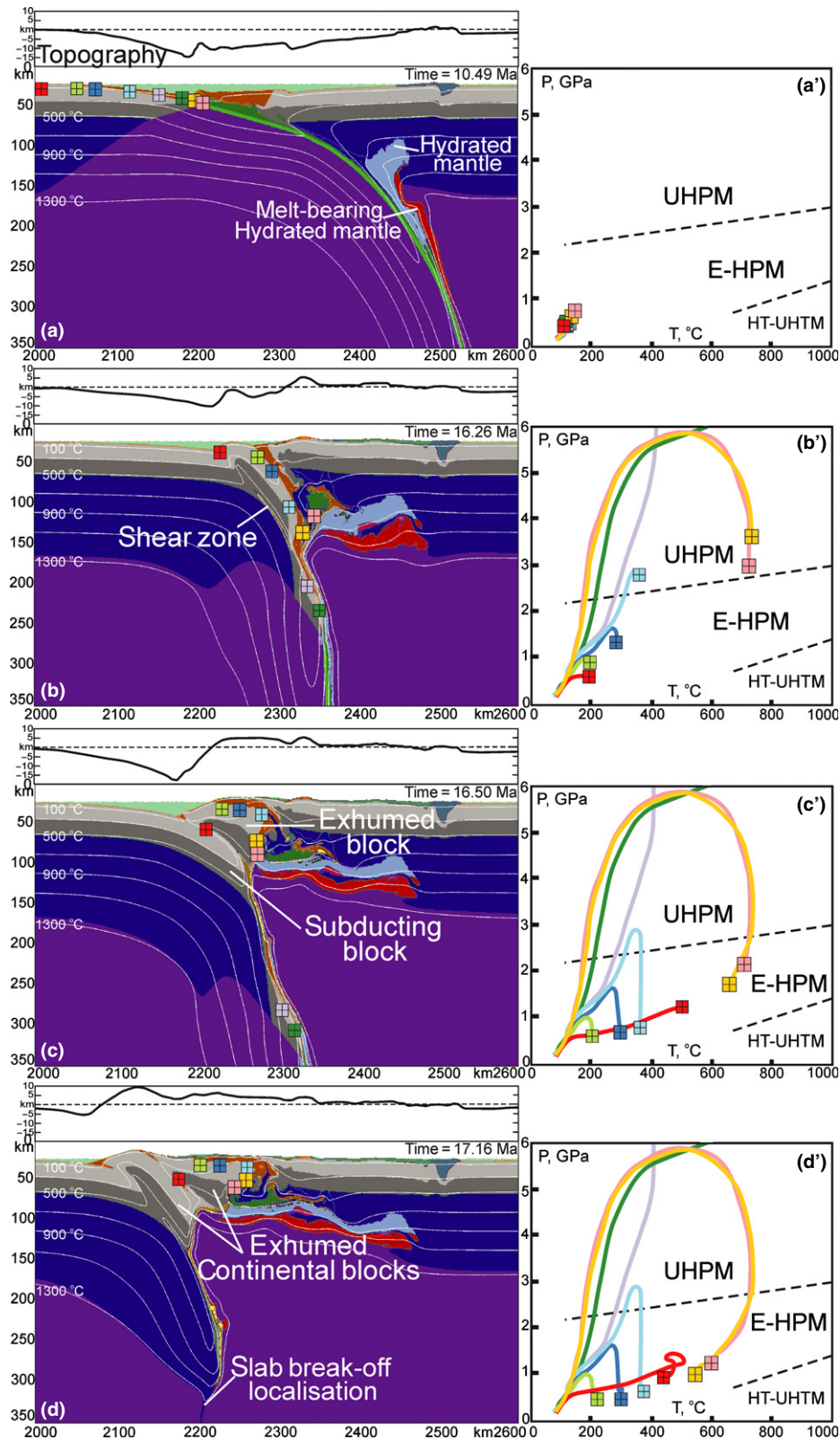


**Fig. 7.** Four time-slice snapshots to show the development of the continental collision zone in model II (left column) and the associated representative  $P$ - $T$ - $t$  paths for crustal rocks (right column).  $600 \times 350$  km sections of the original  $4000 \times 1400$  km model are shown. The topographic profile for each snapshot is given on the top. Coloured squares on the snapshots are markers that refer to the diagrams with the  $P$ - $T$ - $t$  paths (a'-d'). Colour code and notations are the same as in Figs 1 and 4.

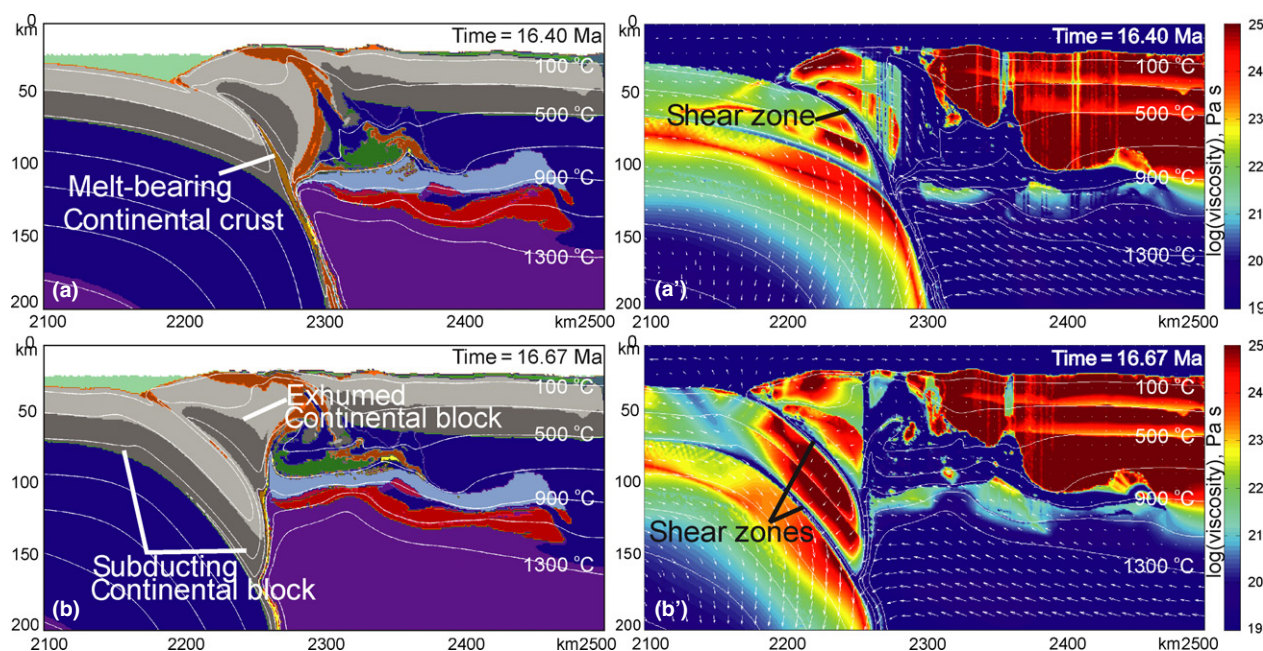


**Fig. 8.** Development of large-scale crustal stacking in model II. Representative  $400 \times 200$  km snapshots (left column) are shown with the respective effective viscosity fields (right column). Colour code in the left column is the same as in Fig. 1. White arrows in the snapshots in the right column show the calculated velocity field; colours represent the magnitude of effective viscosity (see the colour bar). Steeply inclined low viscosity zones between the continental blocks are formed due to the imposed rheological weakening by melts ( $\lambda_{\text{melt}} = 0.001$ ) generated locally as these shear zones develop (see yellow areas in the left column).

shorter segment of oceanic lithosphere produces a reduced length of slab and consequently a weaker slab pull, slower convergence velocity and delayed slab detachment (compare Fig. 3b with Fig. 10c). The reduced slab pull results in relatively shallow subduction of the continental crust to only 80 km depth (Fig. 10b,c) followed by gradual delamination of subducted rocks from the slab and their subsequent exhumation and relamination (underplating) to the base of the overriding plate (cf. Hacker *et al.*, 2011), which is undergoing extension (Fig. 10d). Because the subducted lower continental crust remains in contact with the surrounding hot asthenosphere of the mantle wedge for a prolonged time it undergoes conductive heating up to 800 °C (Fig. 10c) and partial melting at high pressures (near ultrahigh pressures; Fig. 10a'–d'). This provides an additional buoyancy force for ascent of continental plate margin materials to lower crustal-to-middle crustal depths (Fig. 10d' pink, blue and green markers). In general, this shallow crustal relamination process is similar to the ductile crustal extrusion model. An important difference, however, is that extreme HT-UHPM conditions are not reached in the subducted crustal rocks due to the reduced slab pull (compare Fig. 4 with Fig. 10). With a gradual passive margin (150 km wide), model III produces very similar results (Fig. 11a–d) except that the  $P$ – $T$  conditions achieved are slightly more extreme and exhumation involves less decompression but is associated

with slight cooling (compare Fig. 10a'–d' with Fig. 11a'–d').

#### *Model IV: 600 km long oceanic plate with a gradual passive margin*

Figures 12 and 13 represent the evolution of an experiment with the longest oceanic lithosphere component of the left hand plate (600 km), but with the width of the incoming passive margin increased to 150 km (compared with 50 km in model II). The introduction of this gradual passive margin changes the model evolution dramatically (compare Figs 12 & 13 with Figs 6 & 7). The gradual form of the passive margin allows deeper subduction of the continental crust (up to 250 km depth; Figs 12b,c & 13b,c) in comparison with the abrupt form (up to 150 km depth, Figs 6b & 7b).

At a depth of 150–160 km the sedimentary rocks from the deeply subducted passive margin start to ascend, undergo partial melting, and form a diapir above the slab (Fig. 13c,d). This diapir rises vertically penetrating through the lithosphere of the overriding plate weakened by serpentinization during the subduction stage as well as by upward percolation of melts extracted from the diapir. During ascent of the diapir sedimentary rocks mix with hydrated lithospheric mantle of the overriding plate forming a strongly internally deformed UHP melange that is emplaced

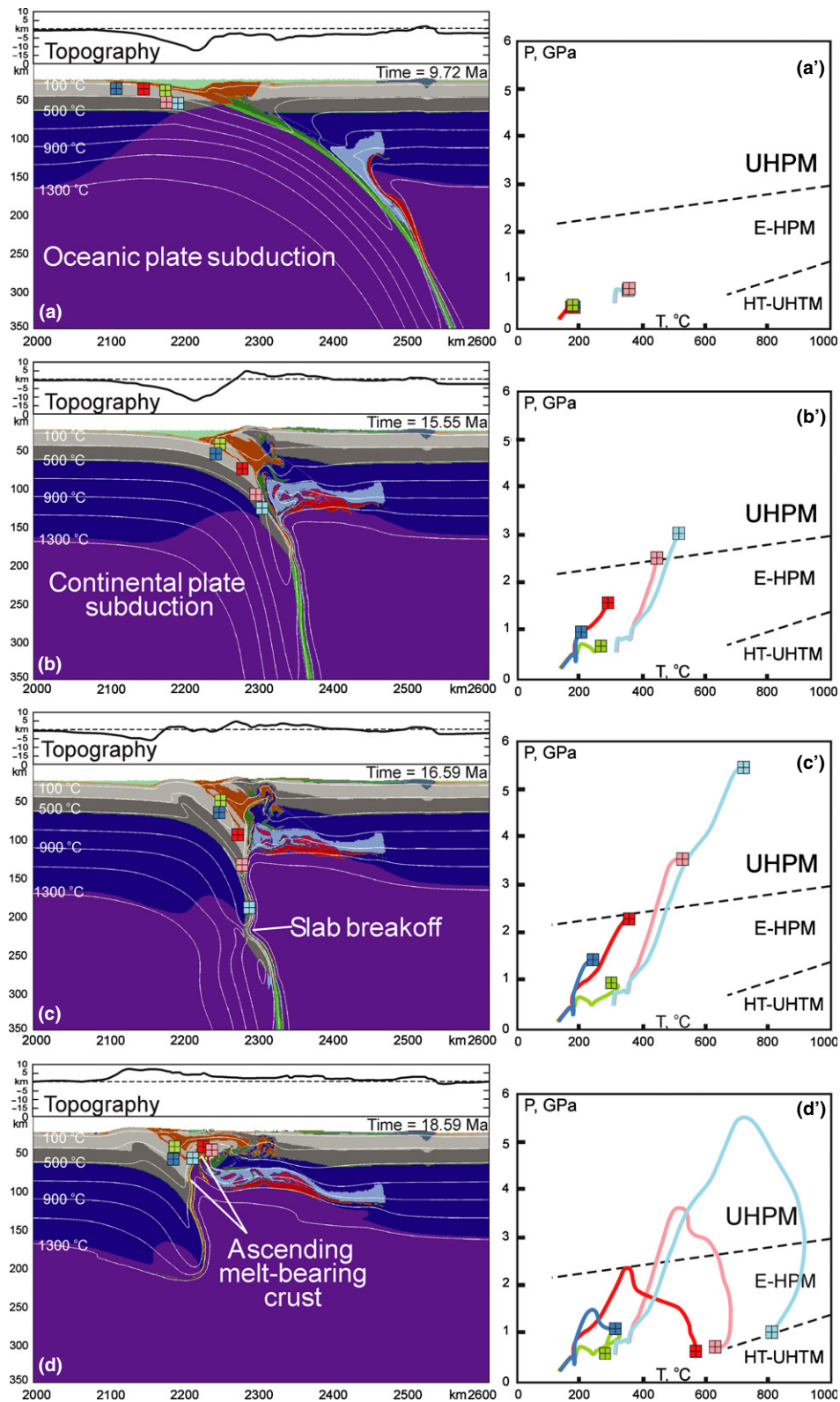


**Fig. 9.** Four time-slice snapshots to show the development of the continental collision zone in a model with a 500 km long oceanic plate and an abrupt passive margin (50 km wide) (left column) and the associated representative  $P$ - $T$ - $t$  paths for crustal rocks (right column).  $600 \times 350$  km sections of the original  $4000 \times 1400$  km model are shown. The topographic profile for each snapshot is given on the top. Coloured squares on the snapshots are markers that refer to the diagrams with the  $P$ - $T$ - $t$  paths (a'-d'). Colour code and notations are the same as in Figs 1 and 4.

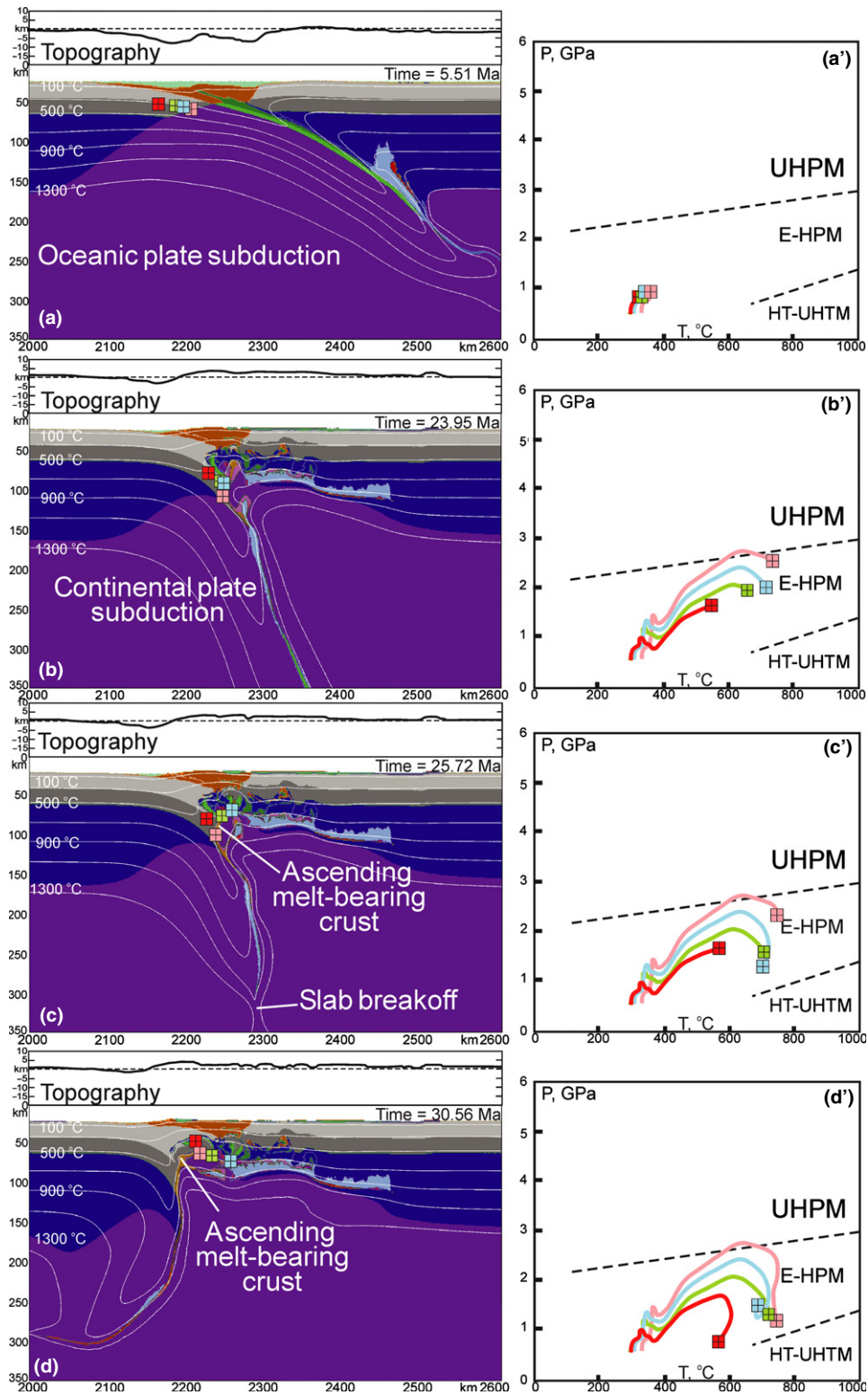


**Fig. 10.** Four time-slice snapshots to show the development of the continental collision zone in model III (shallow crustal delamination) with a 300 km long oceanic plate and an abrupt passive margin (50 km wide) (left column) and the associated representative  $P$ - $T$ - $t$  paths for crustal rocks (right column). 600 × 350 km sections of the original 4000 × 1400 km model are shown. The topographic profile for each snapshot is given on the top. Coloured squares on the snapshots are markers that refer to the diagrams with the  $P$ - $T$ - $t$  paths (a'-d'). Colour code and notations are the same as in Figs 1 and 4.

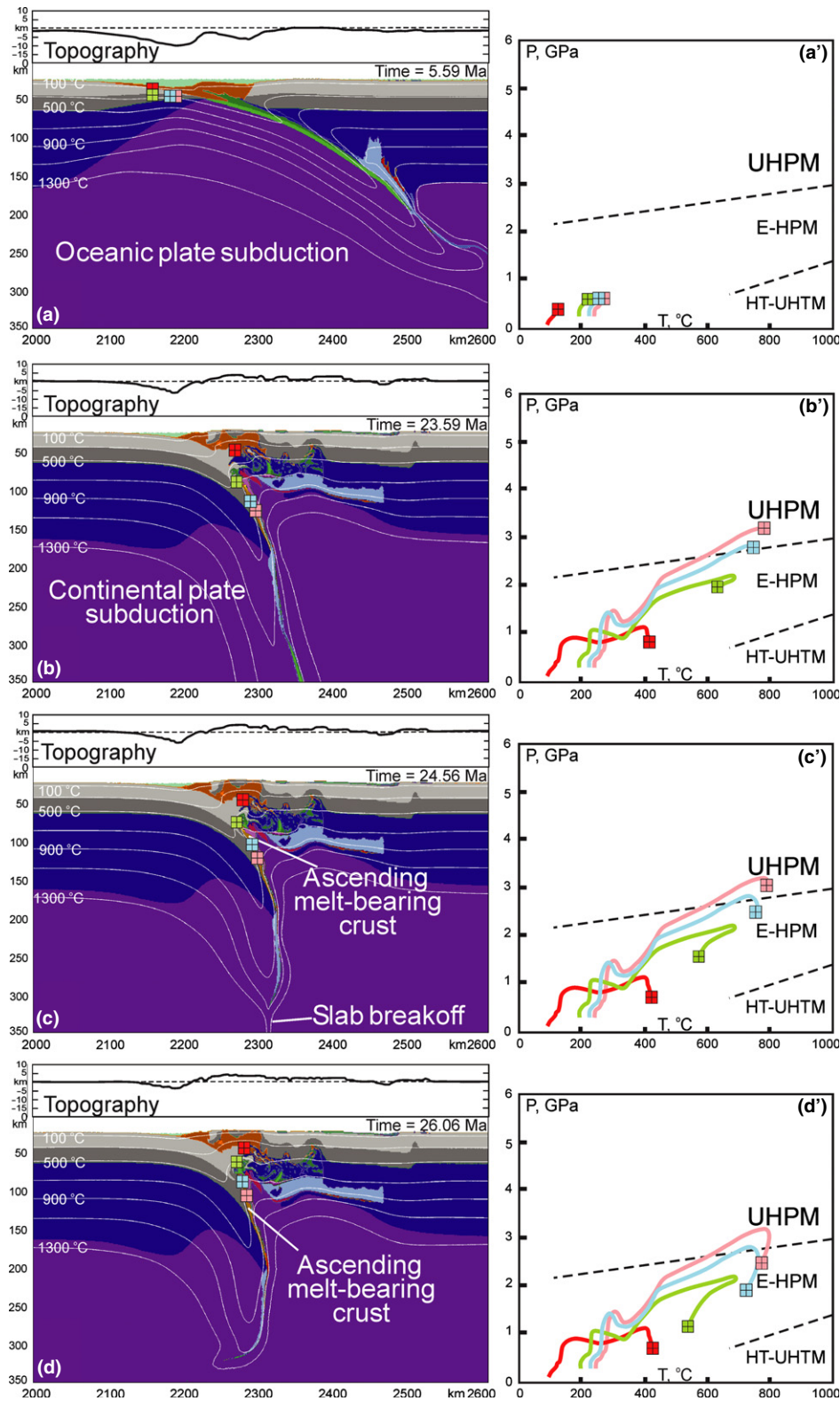


**Fig. 11.** Four time-slice snapshots to show the development of the continental collision zone in model III with a 300 km long oceanic plate and a gradual passive margin (150 km wide) (left column) and the associated representative  $P$ - $T$ - $t$  paths for crustal rocks (right column). 600 × 350 km sections of the original 4000 × 1400 km model are shown. The topographic profile for each snapshot is given on the top. Coloured squares on the snapshots are markers that refer to the diagrams with the  $P$ - $T$ - $t$  paths (a'-d'). Colour code and notations are the same as in Figs 1 and 4.

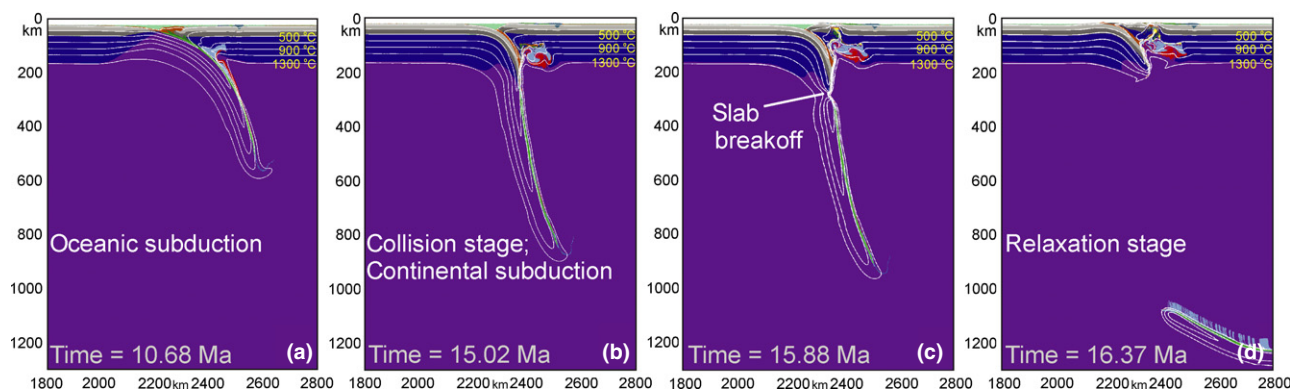


**Fig. 12.** Four time-slice snapshots to show the large-scale evolution of model IV (trans-lithospheric diapirism), which has a 600 km long oceanic plate and a gradual passive margin (150 km wide), up to the relaxation stage.  $1000 \times 1300$  km sections of the original  $4000 \times 1400$  km model are shown. Colour code is the same as in Fig. 1. Detailed development of the collision zone for this model is shown in Fig. 13.

into the bottom of the crust. Similar trans-lithospheric sedimentary diapirs were found in oceanic subduction models when strong melt-induced weakening was implemented (Gerya & Meilick, 2011). The sedimentary materials follow almost isothermal compression and decompression segments in the  $P$ - $T$ - $t$  evolution (Fig. 13a'-d') with maximum temperature not exceeding 700 °C at UHPM conditions (Fig. 13b,b'). With a 500 km long oceanic plate and a gradual passive margin, model IV produces very similar results (Fig. 14a-d) except that multiple diapirs develop, the  $P$ - $T$  paths are more open and higher peak temperature conditions are achieved by the UHPM rocks, and exhumation leads to heating before cooling (compare Fig. 13a'-d' with Fig. 14a'-d').

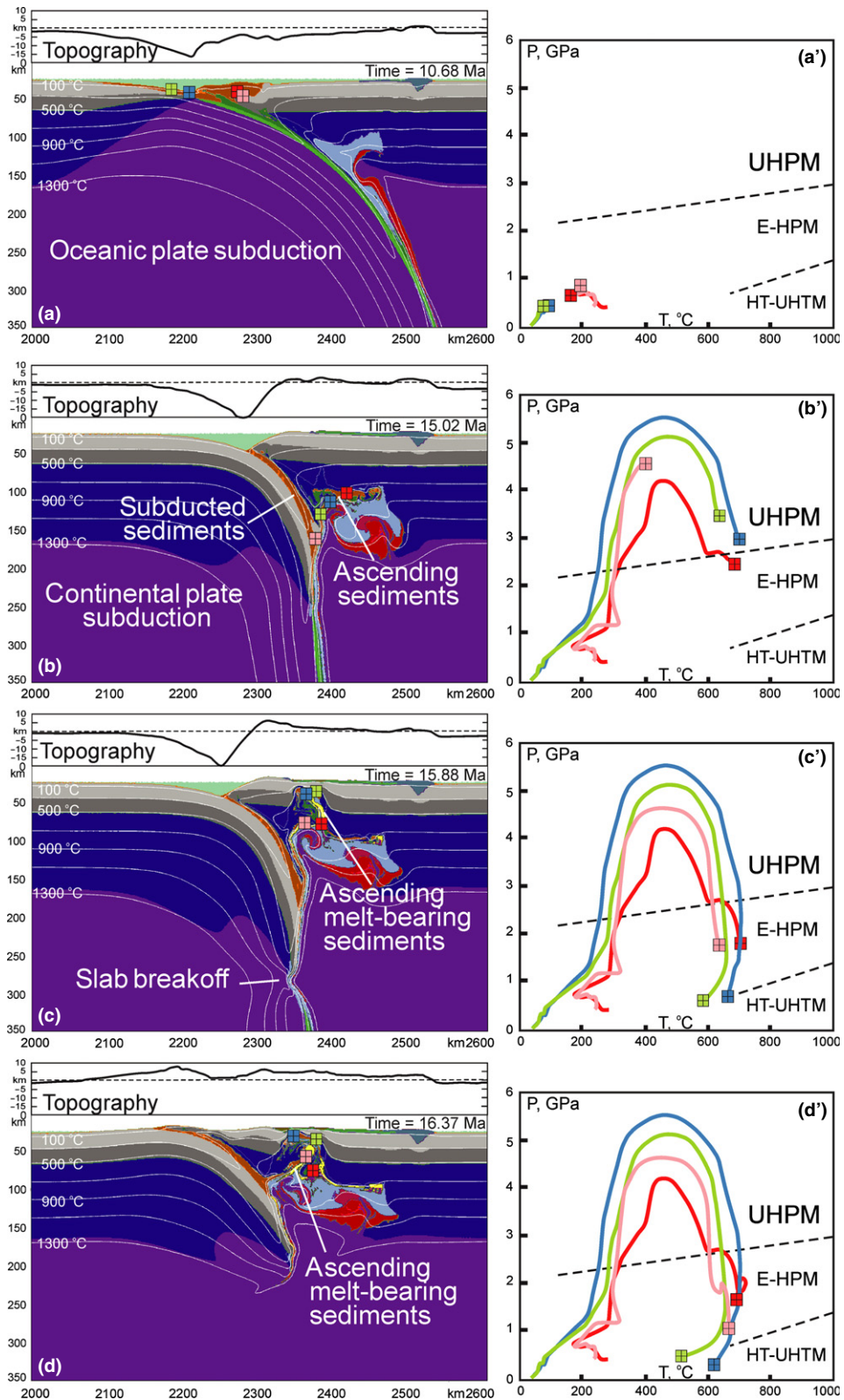
In this study, trans-lithospheric diapirs develop only in models with a gradual passive margin and a relatively long oceanic lithosphere component (500–600 km) on the subducting plate. In the experiments with a shorter length of oceanic lithosphere (300–400 km) the introduction of a gradual passive margin does not produce any significant change in geodynamics. In particular, in the model with an intermediate (400 km) oceanic plate length (Fig. 15) the mode of formation and exhumation of UHPM materials is similar to model I (with an abrupt passive margin producing ductile crustal extrusion). However, the peak metamorphic temperatures and pressures of UHPM rocks are lower (compare Fig. 15b',c' with Fig. 4b',c') and there is a smaller amount of subducted melt-bearing lower continental crust that is extruded in this experiment in comparison with model I (compare Fig. 15b-d with Fig. 4b-d). Similarly, the experiment with a gradual passive margin and the shortest length of oceanic lithosphere (300 km) produces a shallow delamination mode of exhumation (Fig. 11) with a smaller amount of subducted melt-bearing lower continental crust involved in exhumation compared with model III (compare Fig. 11 with Fig. 10).

### Numerical experiment without melting

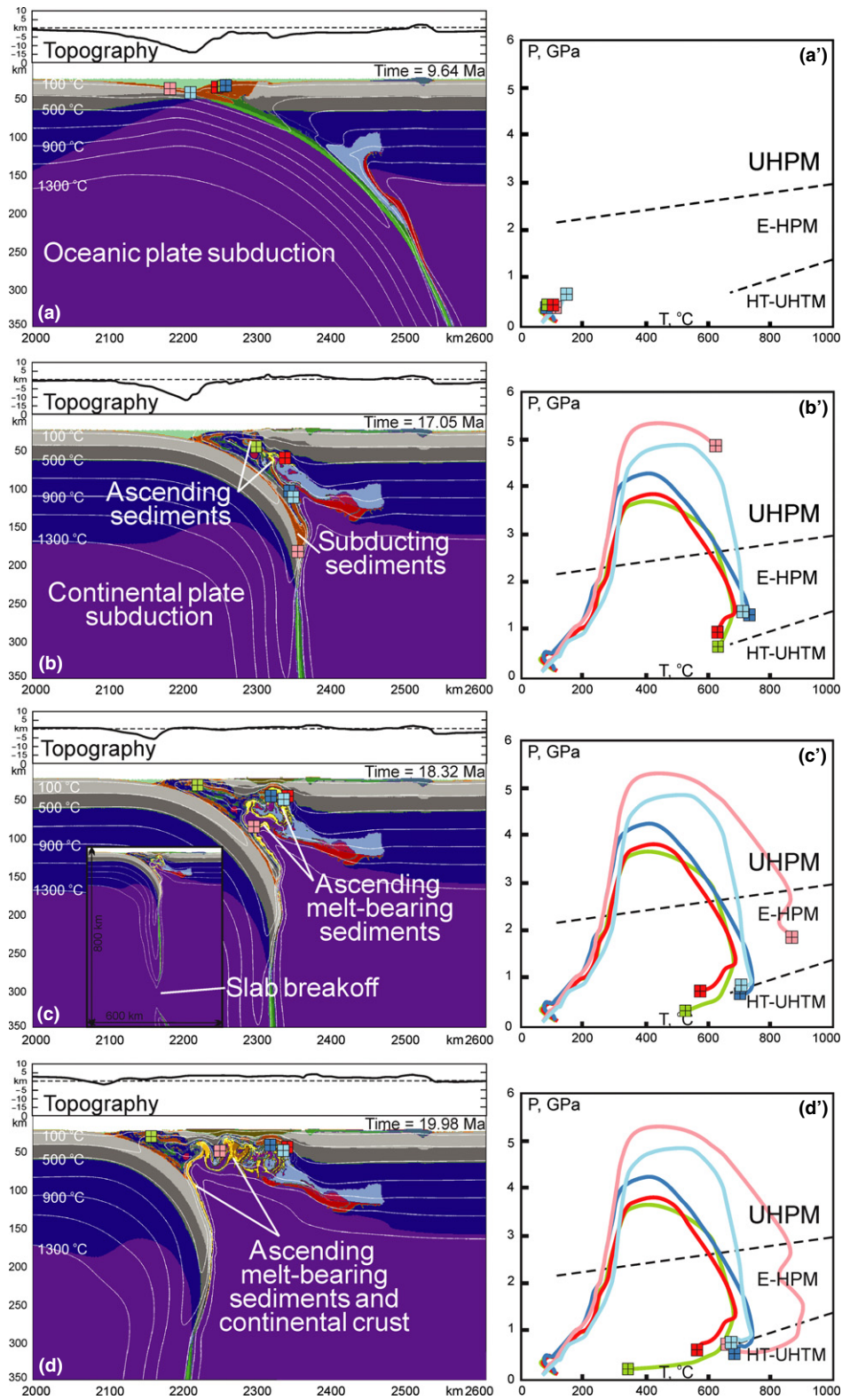
*Model V: 400 km long oceanic plate with an abrupt passive margin*

Figure 16 represents the evolution of an experiment with conditions similar to model I, but in which both hydration and partial melting processes (and related fluid- and melt-induced weakening of rocks) were fully deactivated. The resulting spontaneous collision scenario differs dramatically from model I and demonstrates the typical confined channel flow geometry. Some of the sedimentary materials and the continental crust are subducted into the mantle up to a depth of 120 km (Fig. 16a). Because of the positive buoyancy further subduction of the continental part of the plate is precluded, which leads to slab breakoff in the oceanic part of the plate at a depth of 400 km. After breakoff the continental part of the plate relaxes and the subducted continental crust and sedimentary materials return along the subduction channel towards the surface due to their positive buoyancy (Fig. 16b) simultaneously with partial exhumation of the underlying continental plate (see discussion in Duretz *et al.*, 2011).

The metamorphic evolution for the subducted continental crust and sedimentary materials shows tight  $P$ - $T$ - $t$  paths (Fig. 16a,b'). The maximum  $P$ - $T$  conditions correspond to the transition between the HPM and UHPM fields. The peak temperatures achieved in both the subducted continental crust and the sedimentary materials do not exceed 600 °C (Fig. 16b'). The lower temperatures are in general characteristic for the confined channel flow models where rocks are surrounded by two cold plates. The main reason that this mode of exhumation occurs is the absence of fluid- and melt-induced weakening in the model. As a result, the overriding plate remains rheologically strong during the entire experiment. This, in turn, does not allow for extension of the overriding plate associated with



**Fig. 13.** Four time-slice snapshots to show the development of the continental collision zone in model IV (left column) and the associated representative  $P$ - $T$ - $t$  paths for crustal rocks (right column).  $600 \times 350$  km sections of the original  $4000 \times 1400$  km model are shown. The topographic profile for each snapshot is given on the top. Coloured squares on the snapshots are markers that refer to the diagrams with the  $P$ - $T$ - $t$  paths (a'-d'). Colour code and notations are the same as in Figs 1 and 4.



**Fig. 14.** Four time-slice snapshots to show the development of the continental collision zone in a model with a 500 km long oceanic plate and a gradual passive margin (150 km wide) (left column) and the associated representative  $P$ - $T$ - $t$  paths for crustal rocks (right column). 600 × 350 km sections of the original 4000 × 1400 km model are shown. The topographic profile for each snapshot is given on the top. Coloured squares on the snapshots are markers that refer to the diagrams with the  $P$ - $T$ - $t$  paths (a'-d'). Colour code and notations are the same as in Figs 1 and 4.

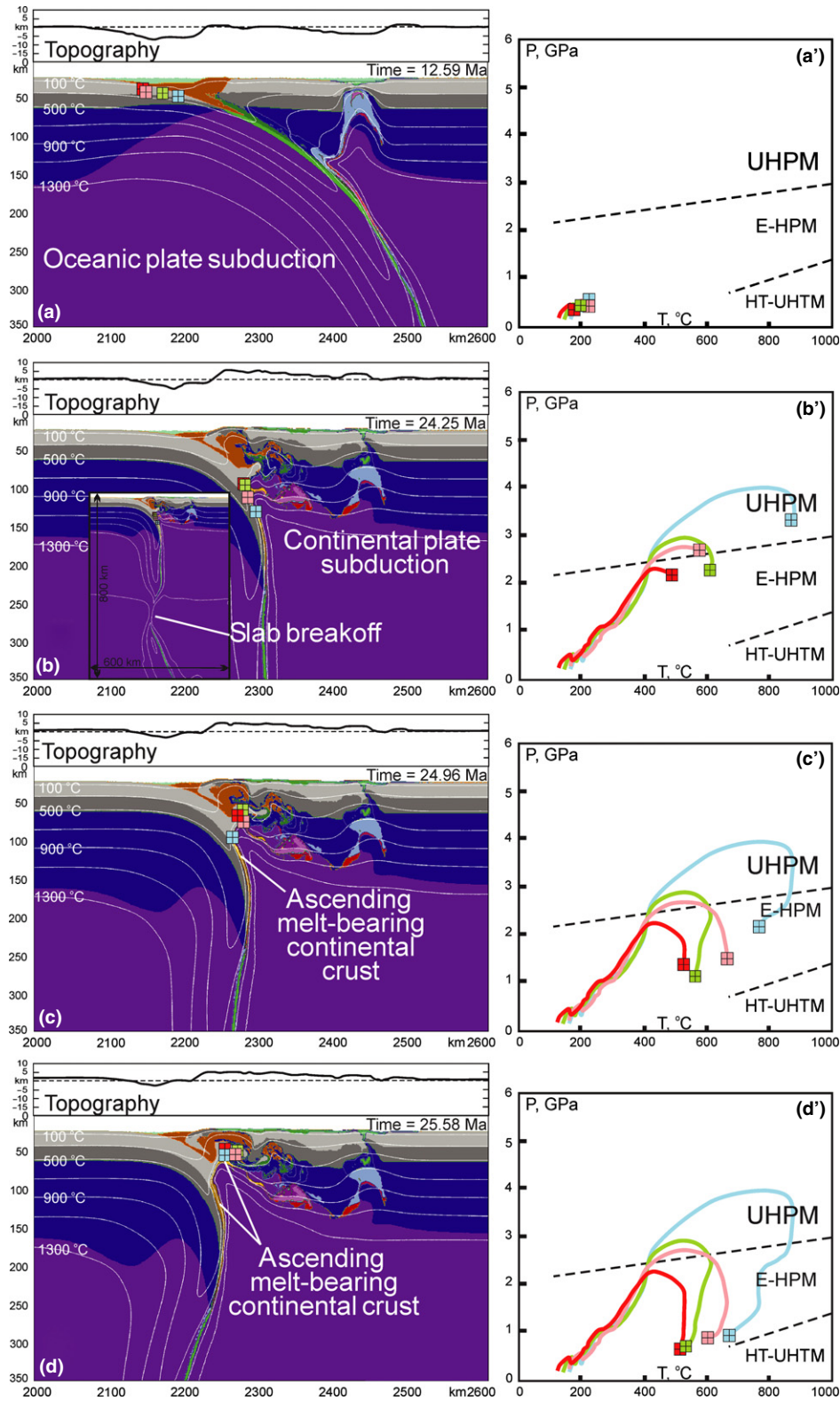


**Fig. 15.** Four time-slice snapshots to show the development of the continental collision zone in a model with a 400 km long oceanic plate and a gradual passive margin (150 km wide) (left column) and the associated representative  $P$ - $T$ - $t$  paths for crustal rocks (right column). 600 × 350 km sections of the original 4000 × 1400 km model are shown. The topographic profile for each snapshot is given on the top. Coloured squares on the snapshots are markers that refer to the diagrams with the  $P$ - $T$ - $t$  paths (a'-d'). Colour code and notations are the same as in Figs 1 and 4.

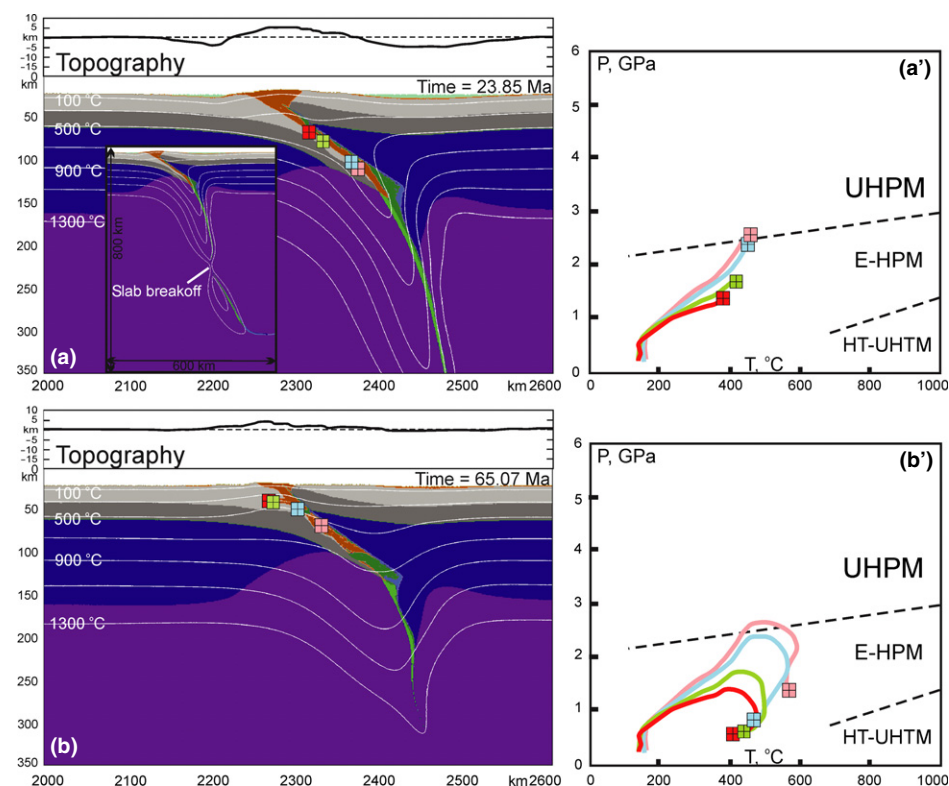


**Fig. 16.** Two time-slice snapshots to show the development of the continental collision zone in model V (channel flow) with a 400 km long oceanic plate and an abrupt passive margin (50 km wide), but with the fluid- and melt-induced weakening deactivated (left column), and the associated representative  $P$ - $T$ - $t$  paths for crustal rocks (right column). 600 × 350 km sections of the original 4000 × 1400 km model are shown. The topographic profile for each snapshot is given on the top. Coloured squares on the snapshots are markers that refer to the diagrams with the  $P$ - $T$ - $t$  paths (a'-d'). Colour code and notations are the same as in Figs 1 and 4.

the ascent of hot asthenospheric mantle or heating of the subducted crustal rocks (e.g. Fig. 4b-d). Therefore, the subduction channel remains confined and strong heating of (U)HPM rocks does not occur.

#### Influence of lower crustal rheology

In all of the models a relatively strong rheology was prescribed for the lower continental crust (plagioclase, An75; Ranalli, 1995), which produced strong coupling along the subducting Moho boundary and enabled deep subduction of the continental crust. To check the influence of lower crustal rheology on the evolution of the models two additional experiments were performed with a weaker lower crustal rheology (wet quartzite; Ranalli, 1995) with the other parameters kept the same as in models I and II. Irrespective of the length of the oceanic plate, these two experiments show a similar evolution with early delamination of the continental crust from the underlying subcontinental lithospheric mantle, which then subducts to great depth (Fig. 17a<sub>1</sub>, b<sub>1</sub>). Deep subduction of the continental crust and the formation of UHPM rocks are precluded in these models of shallow delamination, which to some degree are similar to model III (compare Fig. 17a<sub>2</sub>, b<sub>2</sub> with Fig. 10).

#### DISCUSSION

In the numerical experiments described above, which include fluid- and melt-induced rheological weakening of rocks, the collision stage in the model evolves self-consistently driven by the spontaneous plate convergence velocity and not by a prescribed plate convergence velocity. The results of these novel numerical experiments demonstrate a surprisingly large variety of exhumation mechanisms for UHPM rocks (Fig. 2) ranging from vertical crustal extrusion (model I) and large scale crustal stacking (model II) to shallow crustal delamination (model III) and trans-lithospheric diapirism (model IV) to channel flow and exhumation (model V). These results reconcile well with the variety of exhumation mechanisms for UHPM rocks proposed on the basis of both natural data (e.g. Andersen *et al.*, 1991; Kaneko *et al.*, 2000; Wallis *et al.*, 2005; Epard & Steck, 2008; Brueckner *et al.*, 2010; Hacker *et al.*, 2010; Little *et al.*, 2011) and analogue modelling (e.g. Chemenda *et al.*, 1995). In contrast, a majority of previous numerical models have used a prescribed plate convergence velocity and/or neglected fluid- and melt-induced weakening of rocks. These models consistently demonstrate exhumation of HPM-UHPM materials by various types of channel flow (e.g.

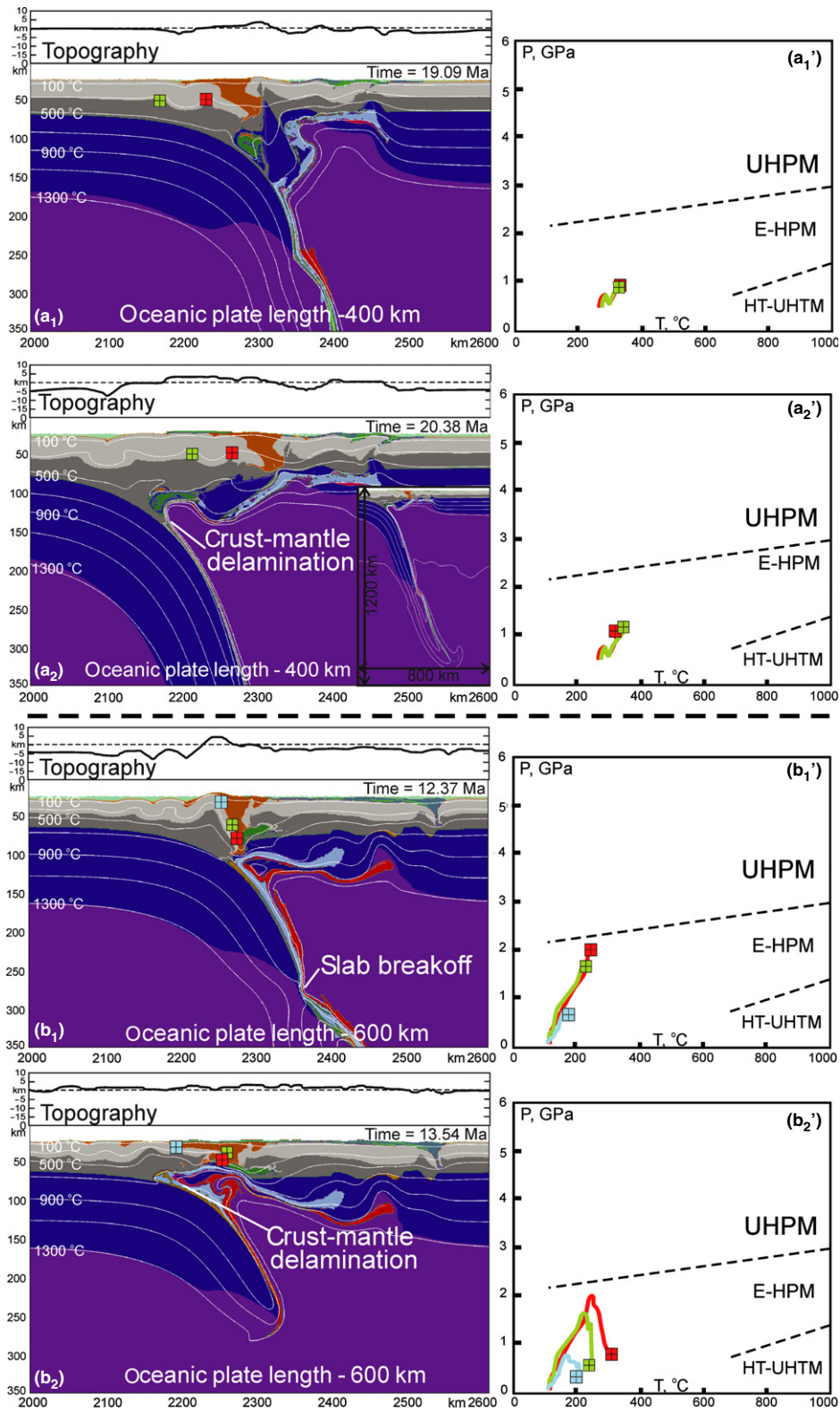


**Fig. 17.** Two time-slice snapshots to show the development of the continental collision zone in models with either a 400 km long (a<sub>1</sub>, a<sub>2</sub>) or a 600 km long (b<sub>1</sub>, b<sub>2</sub>) oceanic plate and an abrupt passive margin (50 km wide, but with a weak lower crustal rheology (left column) and representative  $P$ - $T$ - $t$  paths for crustal rocks (right column). 600 × 350 km sections of the original 4000 × 1400 km model are shown. The topographic profile for each snapshot is given on the top. Coloured squares on the snapshots are markers that refer to the diagrams with the  $P$ - $T$ - $t$  paths (a'-d'). Colour code and notations are the same as in Figs 1 and 4. See text for discussion.

Fig. 16) between confined strong colliding plates (e.g. Burov *et al.*, 2001; Gerya *et al.*, 2008; Warren *et al.*, 2008a,b; Li & Gerya, 2009).

A prescribed convergence velocity driven by plate push is applied widely in numerical models of subduction and collision (e.g. Gerya, 2011 and references therein). This condition is based on the assumption that in a globally confined three-dimensional system of plates, local 'external forcing' imposed on a 2D section of a plate, such as tectonic forces coming from different slabs or from different sections of the same laterally non-uniform slab, can be significant (see discussion in Li & Gerya, 2009). However, prescribing the convergence velocity in numerical models of collision and thus neglecting feedback from the evolving slab pull may inhibit development of several important collisional processes such as slab breakoff, vertical crustal extrusion, large-scale crustal stacking, shallow crustal delamination, trans-lithospheric diapirism and exhumation. The absence of fluid- and melt-related rheological weakening effects in these models is likely to impose similar limitations. Consequently, the significance of channel flow as an exhumation mechanism for UHPM rocks may have been overstated in the literature based on the results of previous numerical experiments.

According to our models with fluid- and melt-induced weakening two major geodynamic parameters are responsible for determining the dominant exhumation mechanism for UHPM rocks during the collision of spontaneously moving plates. These parameters are slab pull and the width (abrupt or gradual geometry) of the subducting continental margin (Fig. 2). Slab pull, in turn, depends on the length and thermal structure of the subducting oceanic plate (e.g. Duretz *et al.*, 2011).

In model I, which has an intermediate length oceanic plate and an abrupt passive margin, after slab breakoff the continental crust is subject to conductive heating as the continental side of the vertically hanging slab comes into contact with the hot asthenosphere of the mantle wedge for sufficient time to allow partial melting of the crust at ultrahigh pressures (Fig. 2c). Partial melting reduces the density and viscosity of the continental crust and triggers exhumation of the buoyant melt-bearing UHPM rocks, which ascend along the slab–mantle interface (Figs 4c,d & 5a,a') by a process of vertical crustal extrusion. The melt-bearing UHPM rocks are exhumed to depths of 10–40 km forming a plume-like body ~50 km across in the lower crust of the extending collision zone in a manner similar to that suggested for the Sulu terrane by Wallis *et al.* (2005). Wallis *et al.* (2005) proposed that partial melting was a key feature in the exhumation of the Sulu UHPM terrane in China and they suggested that the most likely exhumation mechanism for these rocks was diapiric rise of a mobile partially molten mass containing entrained blocks of eclogite. In agreement with nature, the HT-UHPM rocks are found in the

model within high pressure but lower-grade metamorphic units bounded by sharp tectonic contacts ('intrusive-like', e.g. Wang *et al.*, 1997).

In contrast, model II with the longest oceanic plate and an abrupt passive margin (Figs 2a & 7) shows fast stacking of rigid continental crustal blocks, which leads to duplication of the continental crust and the formation of UHPM materials at the frontal part of the suture zone (blue, yellow and pink markers in Fig. 7d,d'). This type of tectonic structure with duplication of the continental crust by intracontinental thrusting associated with coeval erosion is documented for several collisional orogenic systems, such as, for example, the western Alps in Europe (Schmidt & Kissling, 2000), the Dabie Shan in China (Okay & Sengör, 1992; Okay *et al.*, 1993; Yin & Nie, 1993; Nie *et al.*, 1994) and the Western Gneiss Region in Norway (Hacker *et al.*, 2010). Okay & Sengör (1992) argued that major intracontinental thrusting with concomitant erosion and associated back thrusting were the main factors in the initial exhumation of UHPM rocks in the Dabie Shan complex in China. They interpreted a stack of several major tectonic units separated by intracontinental thrusts south of the Qinling suture as a pop-up structure, and argued that the driving force for intracontinental thrusting was initially the post-collisional negative buoyancy-driven convergence between the Sino-Korean and Yangtze plates generated by the descending lithospheric root, whereas final exhumation was consequent upon detachment of the lithospheric root. Similar subparallel thrusts were observed in model II where large coherent crustal-scale blocks of continental crust become detached from the subducting subcontinental lithospheric mantle and are thrust back over the subducting plate along a major shear zone, which exhumes the UHPM rocks to lower-to-middle crustal depths. The uplift of the subducted crustal blocks and the fast exhumation of the UHPM rocks are similar to the results of analogue modelling, which was successfully applied to the Himalayas and other zones of continental subduction (Chemenda *et al.*, 1995, 2000).

The mechanism of wedge extrusion induced by detachment of the deeply subducted crustal materials from the downgoing plate and subsequent upward motion, as proposed by many authors (e.g. van den Beukel, 1992; Okay *et al.*, 1993; Ernst & Liou, 1995; Kaneko *et al.*, 2000; Smye *et al.*, 2010), has similarities with the results of experiments using a numerical model with a 500 km long oceanic plate and an abrupt passive margin (Figs 2b & 9). As an example, Kaneko *et al.* (2000) proposed a wedge extrusion model for the Kokchetav HP–UHPM belt, based on detailed mapping and an extensive structural dataset. They showed that the crustal protoliths for the UHPM rocks were subducted to depths of over 200 km before being extruded back to crustal depths. The tectonic unit with the HP–UHPM rocks is bound by subhorizontal faults and now occurs in a sandwich-like structure between

underlying low pressure metamorphic rocks and overlying weakly or unmetamorphosed rocks. This example is in good agreement with the model results, where the continental rocks were subducted to a depth of 180 km before exhumation to middle crustal depths within high pressure but lower-grade metamorphic units (Fig. 9). The results of this experiment are similar to the results from the model II, but in this case only a single episode of crustal stacking or wedge extrusion occurs due to the reduced slab pull.

In other experiments with the longest oceanic plate, but with a gradual passive margin rather than an abrupt passive margin (model IV), exhumation of deeply subducted crustal and sedimentary materials, which undergo partial melting at UHPM conditions, occurs by trans-lithospheric diapiric flow (Figs 2e,f, 13 & 14). Cloos (1993) was the first to suggest that deeply subducted continental crust can warm, decouple from its mantle root, and rise diapirically, driven upward by a density contrast with the overlying mantle of  $0.50 \text{ g cm}^{-3}$  or more. Such a mechanism has been proposed for UHPM rocks in the North Qaidam UHPM belt in the Northern Tibetan Plateau of Northwest China in the Ordovician–Silurian (Yin *et al.*, 2007), in the Norwegian Caledonides in the Lower Devonian (Root *et al.*, 2005), in the Dabie Shan, eastern China in the Triassic (Wang & Cong, 1999), in the southeastern Pamir in the Eocene–Miocene (Hacker *et al.*, 2005) and in the D'Entrecasteaux Islands, Papua New Guinea in the Miocene–Pliocene (Little *et al.*, 2011), and is expected to occur in many arcs (Behn *et al.*, 2011). For the North Qaidam UHPM belt, Yin *et al.* (2007) proposed that after reaching UHPM conditions the subducted materials were transported across the mantle wedge in diapirs originating from a melange channel above the subducting plate and emplaced into the base of a coeval magmatic arc. In model IV, the prescribed melt-related weakening associated with formation of the arc creates a weak zone within the mantle wedge promoting exhumation of the UHPM rocks by diapiric flow from the subduction channel through the mantle wedge followed by emplacement into the lower arc crust (Figs 13 & 14).

Experiments in which the length of the oceanic plate is short produce a weaker slab pull, slower convergence velocity and delayed slab detachment (Fig. 10c). The reduced slab pull results in a relatively shallow continental subduction followed by gradual delamination of subducted rocks from the slab and their subsequent relamination (cf. Hacker *et al.*, 2011) to the extending overriding plate (Fig. 10d). Because the subducted lower continental crust remains in contact with the surrounding hot asthenosphere of the mantle wedge for a prolonged time it undergoes conductive heating up to  $800 \text{ }^\circ\text{C}$  (Fig. 10c) – to slightly higher temperatures with a gradual passive margin – and partial melting at high pressures – even at ultrahigh pressures with a gradual passive margin (Fig. 2d,h). In many

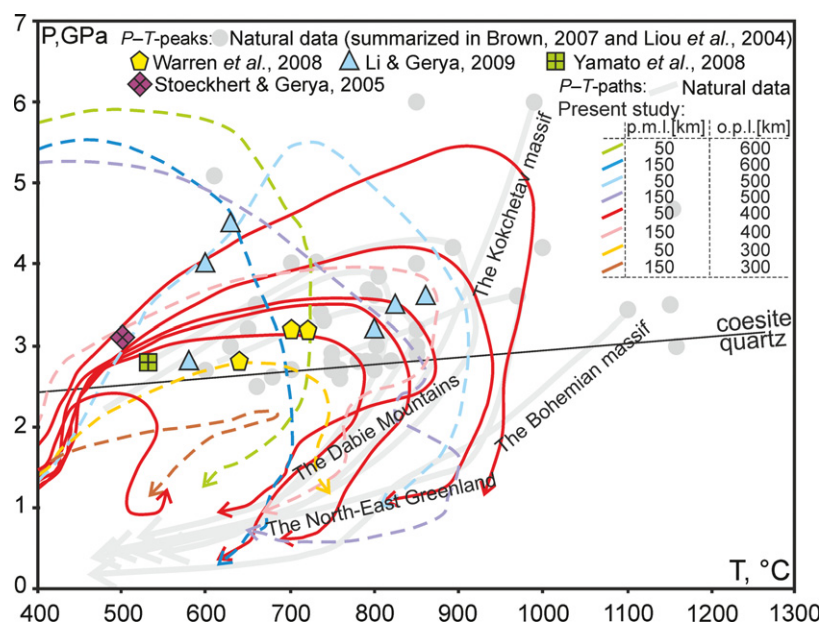
respects, this shallow crustal relamination process is similar to the vertical crustal extrusion mechanism, which occurs in model I, except that the  $P$ – $T$  conditions achieved are not as extreme.

The numerical experiment without fluid- and melt-induced weakening illustrates a typical example of the channel flow mechanism for exhumation of HPM–UHPM rocks (Fig. 16), which has been suggested by many authors, such as for example, Mancktelow (1995), Dobretsov (2000), Burov *et al.* (2001), Gerya *et al.* (2008), Li & Gerya (2009) and Warren *et al.* (2008a,b). The peak temperatures achieved in the exhumed materials do not exceed  $600 \text{ }^\circ\text{C}$ , which is in good agreement with previous channel flow models (e.g. Warren *et al.*, 2008a,b; Yamato *et al.*, 2008). However, evidence of partial melting has been documented from many UHPM terranes worldwide (e.g. Andersen & Osmundsen, 1994; Zhong *et al.*, 2001; Labrousse *et al.*, 2002, 2011; Hacker *et al.*, 2005; Wallis *et al.*, 2005; Lang & Gilotti, 2007; Ragozin *et al.*, 2009; Zeng *et al.*, 2009; Zheng *et al.*, 2011; Gao *et al.*, 2012; ) and is a typical feature associated with exhumation of UHPM rocks. For some of the models discussed above, partial melting triggers ductile ascent of the crustal and sedimentary materials to mid-to-lower crustal depths (Figs 4 & 5), which may also be responsible for the formation of tectonic contacts between UHPM rocks and the surrounding units. Tectonic contacts between units are commonly reported from UHPM terranes (e.g. Wang *et al.*, 1997; Avigad *et al.*, 2003; Faure *et al.*, 2003; Epard & Steck, 2008) and are also seen in the geodynamical models of Beaumont *et al.* (2009).

Another important parameter that contributes to the exhumation of continental rocks subducted to mantle conditions is erosion. Removing material at the surface by erosion may facilitate uplift along steep faults and thus affect the style of exhumation. Erosion is invoked to explain exhumation in many natural collision zones (e.g. Pfiffner *et al.*, 2000; Burbank, 2002; Vance *et al.*, 2003; Cederbom *et al.*, 2004; Wittmann *et al.*, 2007; Champagnac *et al.*, 2008). In this study, we did not concentrate on the final exhumation of the subducted crustal rocks to the surface from lower-to-middle crustal depths, which indeed could be realized by erosion or younger tectonic events. Nevertheless the upper boundary in our experiments evolves by erosion and sedimentation with relatively low rates of  $0.03 \text{ mm year}^{-1}$ , as explained in the description of the model design above. Increasing these rates up to  $10 \text{ mm year}^{-1}$  in accordance with some estimates from natural collision zones (e.g. Burbank, 2002) is likely to result in faster exhumation of UHPM rocks in the experiments that generated high topography (e.g. Figs 4, 7 & 13).

The  $P$ – $T$ – $t$  paths recorded by markers in experiments with model I (red lines on Fig. 18) reproduce well the  $P$ – $T$ – $t$  paths recorded by UHPM rocks in the geological record. The narrow  $P$ – $T$ – $t$  loops are similar

**Fig. 18.** Summary of observed and predicted  $P$ – $T$  conditions for UHPM units. Grey symbols represent peak  $P$ – $T$  conditions retrieved from single rock samples from various UHPM terranes (thermobarometry summarized in Liou *et al.*, 2004 and Brown, 2007; and with additional data from Carswell, 1991 and Wang & Cong, 1999), whereas coloured symbols represent peak  $P$ – $T$  conditions predicted by numerical modelling experiments (Stoekert & Gerya, 2005; Warren *et al.*, 2008a; Yamato, 2008; Li & Gerya, 2009).  $P$ – $T$ – $t$  paths retrieved from various UHPM terranes, including the Dabie-Shan (Wang & Cong, 1999), North-East Greenland (Gilotti & McClelland, 2007), the Kokchetav massif (Liou *et al.*, 2004), and the Bohemian massif (Carswell, 1991) are shown in grey.  $P$ – $T$ – $t$  paths from the models discussed in this paper are shown in colour, with the  $P$ – $T$ – $t$  paths from model I shown in red solid lines, whereas the  $P$ – $T$ – $t$  paths for maximum  $P$ – $T$  conditions for other experiments are shown as coloured dashed lines.



to those retrieved from the Dabie Shan UHPM rocks, whereas the wide  $P$ – $T$ – $t$  loops show some similarities with the decompression pattern of the North-East Greenland UHPM rocks. Also, within a single model, crustal and sedimentary materials are exhumed from various depths and record different decompression paths—features that are similar to those retrieved from some UHPM complexes, for example in the Dabie Shan (e.g. Wang & Cong, 1999). The average exhumation rate to crustal depths for the melt-bearing UHPM materials in model I is  $\sim 4.5 \text{ cm year}^{-1}$  (Fig. 4b–d). This rate is similar to the fastest exhumation rates determined for the initial exhumation of UHPM rocks to crustal depths, which are in the range of  $1\text{--}8 \text{ cm year}^{-1}$  (Hermann *et al.*, 2001; Rubatto & Hermann, 2001; Root *et al.*, 2005; Parrish *et al.*, 2006) demonstrating that exhumation can take place at plate tectonic velocities similar to subduction.

The experimental results from the numerical models in this study (Figs 2 & 18) cover a larger proportion of the range of  $P$ – $T$  conditions documented from UHPM rocks than the results of experiments from previous numerical models, and in particular the results reproduce HT–UHPM  $P$ – $T$  conditions. Nonetheless, some extreme temperature conditions that have been suggested for the Kokchetav and Bohemian massifs, perhaps up to  $1100\text{--}1200 \text{ °C}$  (Massonne, 2003), are still to be achieved in experiments using numerical models. Also, to better constrain the input parameters for models of exhumation of HT–UHPM rocks there is a need for detailed description of the evidence for partial melting and for the interpretation of melting processes, as well as for better information about the rheological behaviour of melt-bearing rocks at UHPM conditions. The scattering of peak  $P$ – $T$  conditions for natural UHPM rocks is quite large—temperature

variation is from  $600$  to  $1150 \text{ °C}$  and pressure variation is from  $2.5$  to  $6 \text{ GPa}$  (Fig. 18). Previous numerical models (e.g. Gerya *et al.*, 2008; Warren *et al.*, 2008a,b; Yamato *et al.*, 2008) have not reproduced the full variation in  $P$ – $T$  conditions and mainly achieve lower-temperature conditions for the formation of UHPM rocks (commonly up to  $700 \text{ °C}$ ). Only one recent model (Li & Gerya, 2009) predicts higher temperatures (up to  $860 \text{ °C}$ ) for UHPM rocks, in this case in sublithospheric plumes that are exhumed toward the surface within the subduction channel. One possible explanation for these discrepancies may be related to the using of a prescribed rather than a spontaneous plate convergence velocity condition that favours channel flow in a confined plate interface and precludes prolonged thermal interaction of the hot asthenospheric mantle with the subducted crustal rocks at UHPM conditions.

## CONCLUSIONS

Results of 2D petrological–thermomechanical numerical experiments demonstrate a broad variability of exhumation mechanisms for UHPM rocks during collision of spontaneously moving plates. Five distinct modes of exhumation of (U)HPM rocks were identified in the models associated with different collision scenarios in terms of the length of the subducted oceanic plate (from  $300$  to  $600 \text{ km}$ ) and the form of the passive margin (either  $50$  or  $150 \text{ km}$  wide): vertical crustal extrusion, large-scale crustal stacking, shallow crustal delamination, trans-lithospheric diapirism, and channel flow.

The range of exhumation mechanisms for (U)HPM rocks for collision models with spontaneous moving plates revealed in this study is in contrast with the

domination of channel flow mechanisms in many of the collision models that used a prescribed plate convergence velocity and/or neglected fluid- and melt-induced weakening of rocks. This suggests that the prescribed convergence velocity driven by the plate push in previous numerical models of collision may inhibit development of several important processes, such as slab breakoff and exhumation as well as crustal delamination and large-scale stacking of crustal blocks. Neglect of fluid- and melt-related weakening effects in these models is likely to impose similar limitations. Consequently, the significance of channel flow for the exhumation of UHPM rocks may be overstated in the literature based on the results of these earlier numerical experiments.

Furthermore, the results from this study cover a larger proportion of the full range of  $P$ – $T$  conditions documented from UHPM rocks, particularly for HT–UHPM rocks, than the results of experiments from previous numerical models with a prescribed plate convergence velocity. The highest peak metamorphic temperatures (up to 1000 °C) are recorded in the case of vertical crustal extrusion (model I) in which subducted continental crust is subject to prolonged conductive heating due to contact between the asthenospheric mantle and the continental crust of the vertically hanging slab. Nonetheless, some extreme temperature conditions which have been suggested for the Kokchetav and Bohemian massifs, perhaps up to 1100–1200 °C, are still to be achieved in experiments using numerical models.

#### ACKNOWLEDGEMENTS

The authors thank A. Pfiffner and an anonymous reviewer for their constructive comments on the original manuscript. This work was supported by ETH Research Grants TH-12/05-3 and TH-0807-3, and SNF Research Grants 200021-113672/1 and 200021-116381/1.

#### REFERENCES

- Andersen, T.B. & Jamtveit, B., 1990. Uplift of deep crust during orogenic extensional collapse—a model based on field studies in the Song-Sunnfjord region of western Norway. *Tectonics*, **9**, 1097–1111.
- Andersen, T.B. & Osmundsen, P.T., 1994. Deep crustal fabrics and a model for the extensional collapse of the southwest Norwegian Caledonides. *Journal of Structural Geology*, **16**, 1191–1203.
- Andersen, T.B., Jamtveit, B. & Dewey, J.F., 1991. Subduction and exhumation of continental crust: major mechanisms during continent–continent collision and orogenic extensional collapse, a model based on the south Norwegian Caledonides. *Terra Nova*, **3**, 303–310.
- Auzanneau, E., Vielzeuf, D. & Schmidt, M.W., 2006. Experimental evidence of decompression melting during exhumation of subducted continental crust. *Contributions to Mineralogy and Petrology*, **152**, 125–148.
- Avigad, D., Chopin, C. & Le Bayon, R., 2003. Thrusting and extension in the southern Dora-Maria ultra-high-pressure massif (Western Alps); view from below the coesite-bearing unit. *Journal of Geology*, **111**, 57–70.
- Baumann, C., Gerya, T. & Connolly, J.A.D., 2010. Numerical modelling of spontaneous slab breakoff dynamics during continental collision. In: *Advances in Interpretation of Geological Processes* (eds Spalla, M.I., Marotta, A.M. & Gosso, G. eds). *Geological Society, London, Special Publications*, **332**, 99–114.
- Beaumont, C., Jamieson, R.A., Butler, J.P. & Warren, C.J., 2009. Crustal structure: a key constraint on the mechanism of ultra-high-pressure rock exhumation. *Earth and Planetary Science Letters*, **287**, 116–129.
- Behn, M.D., Kelemen, P.B., Hirth, G., Hacker, B.R. & Massonne, H.-J., 2011. Diapirs as the source of the sediment signature in arc lavas. *Nature Geoscience*, **4**, 641–646.
- Bittner, D. & Schmeling, H., 1995. Numerical modeling of melting processes and induced diapirism in the lower crust. *Geophysical Journal International*, **123**, 59–70.
- Boutelier, D., Chemenda, A. & Jorand, C., 2004. Continental subduction and exhumation of high-pressure rocks: insight from thermo-mechanical laboratory modelling. *Earth and Planetary Science Letters*, **222**, 209–216.
- Brown, M., 2007. Metamorphic conditions in orogenic belts: a record of secular change. *International Geology Review*, **49**, 193–234.
- Brueckner, H.K., Carswell, D.A., Griffin, W.L., Medaris, L.G., Van Roermund, H.L.M. & Cuthbert, S.J., 2010. The mantle and crustal evolution of two garnet peridotite suites from the Western Gneiss Region, Norwegian Caledonides: an isotopic investigation. *Lithos*, **117**, 1–19.
- Brun, J.-P. & Faccenna, C., 2008. Exhumation of high-pressure rocks driven by slab rollback. *Earth and Planetary Science Letters*, **272**, 1–7.
- Burbank, D.W., 2002. Rates of erosion and their implications for exhumation. *Mineralogical Magazine*, **66**, 25–52.
- Burg, J.-P. & Gerya, T.V., 2005. The role of viscous heating in Barrovian metamorphism of collisional orogens: thermomechanical models and application to the Lepontine Dome in the Central Alps. *Journal of Metamorphic Geology*, **23**, 75–95.
- Burov, E., Jolivet, L., Le Pourhiet, L. & Poliakov, A., 2001. A thermomechanical model of exhumation of high pressure (HP) and ultra-high pressure (UHP) metamorphic rocks in Alpine-type collision belts. *Tectonophysics*, **342**, 113–136.
- Butler, J.P., Beaumont, C. & Jamieson, R.A., 2011. Crustal emplacement of exhuming (ultra)high-pressure rocks: will that be pro- or retro-side? *Geology*, **39**, 635–638.
- Carswell, D.A., 1991. Variscan high  $P$ – $T$  metamorphism and uplift history in the Moldanubian zone of the Bohemian Massif, Lower Austria. *European Journal of Mineralogy*, **3**, 323–342.
- Cederbom, C.E., Sinclair, H.D., Schlunegger, F. & Rahn, M.K., 2004. Climate-induced rebound and exhumation of the European Alps. *Geology*, **32**, 709–712.
- Champagnac, J.-D., Van Der Beek, P., Diraison, G. & Dauphin, S., 2008. Flexural isostatic response of the Alps to increased Quaternary erosion recorded by foreland basin remnants, SE France. *Terra Nova*, **20**, 213–220.
- Chemenda, A.I., Mattauer, M., Malavieille, J. & Bokun, A.N., 1995. A mechanism for syn-collisional rock exhumation and associated normal faulting: results from physical modelling. *Earth and Planetary Science Letters*, **132**, 225–232.
- Chemenda, A.I., Burg, J.P. & Mattauer, M., 2000. Evolutionary model of the Himalaya-Tibet system: geopoem based on new modelling, geological and geophysical data. *Earth and Planetary Science Letters*, **174**, 397–409.
- Chopin, C., 1984. Coesite and pure pyrope in high-grade blueschists of the western Alps: a first record and some consequences. *Contributions to Mineralogy and Petrology*, **86**, 107–118.
- Chopin, C., 2003. Ultrahigh pressure metamorphism: tracing continental crust into the mantle. *Earth and Planetary Science Letters*, **212**, 1–14.

- Clauser, C. & Huenges, E., 1995. Thermal conductivity of rocks and minerals. In: *Rock Physics and Phase Relations* (ed. Ahrens, T.J.). *AGU Reference Shelf*, **3**, 105–126.
- Cloos, M., 1993. Lithospheric buoyancy and collisional orogenesis: subduction of oceanic plateau, continental margins, island arcs, spreading ridges, and seamounts. *Geological Society of America Bulletin*, **105**, 715–737.
- Connolly, J.A.D., 2005. Computation of phase equilibria by linear programming: a tool for geodynamic modelling and its application to subduction zone decarbonation. *Earth and Planetary Science Letters*, **236**, 524–541.
- Dewey, J.F., Ryan, P.D. & Andersen, T.B., 1993. Orogenic uplift and collapse, crustal thickness, fabrics, and metamorphic phase changes: the role of eclogites. In: *Magmatic Processes and Plate Tectonics* (eds Prichard, H.M., Alabaster, T., Harris, N.B.W. & Neary, C.R.). *Geological Society, London, Special publication*, **76**, 325–343.
- Djomani, Y.H.P., O'Reilly, S.Y., Griffin, W.L. & Morgan, P., 2001. The density structure of subcontinental lithosphere through time. *Earth and Planetary Science Letters*, **184**, 605–621.
- Dobretsov, N.L., 2000. Collision processes in Paleozoic fold-belts of Asia and exhumation mechanisms. *Petrology*, **8**, 403–427.
- Duret, T., Gerya, T.V. & May, D.A., 2011. Numerical modelling of spontaneous slab breakoff and subsequent topographic response. *Tectonophysics*, **502**, 244–256.
- Elliott, T., Plank, T., Zindler, A., Wjite, W. & Bourdon, B., 1997. Element transport from slab to volcanic front at the Mariana arc. *Journal of Geophysical Research*, **102**, 14991–15019.
- Epard, J.L. & Steck, A., 2008. Structural development of the Tso Moriri ultra-high pressure nappe of the Ladakh Himalaya. *Tectonophysics*, **451**, 242–264.
- Ernst, W.G., 2001. Subduction, ultrahigh-pressure metamorphism, and regurgitation of buoyant crustal slices—implications for arcs and continental growth. *Physics of the Earth and Planetary Interiors*, **127**, 253–275.
- Ernst, W.G. & Liou, J.G., 1995. Contrasting plate tectonic styles of the Qinling-Dabie-Sulu and Franciscan metamorphic belts. *Geology*, **23**, 253–256.
- Faccenda, M., Gerya, T.V. & Chakraborty, S., 2008. Styles of post-subduction collisional orogeny: influence of convergence velocity, crustal rheology and radiogenic heat production. *Lithos*, **103**, 257–287.
- Faure, M., Lin, W., Scharer, U., Shu, L.S., Sun, Y. & Arnaud, N., 2003. Continental subduction and exhumation of UHP rocks. Structural and geochemical insights from the Dabiehan (East China). *Lithos*, **70**, 213–241.
- Gao, X.-Y., Zheng, Y.-F. & Chen, Y.-X., 2012. Dehydration melting of ultrahigh-pressure eclogite in the Dabie orogen: evidence from multiphase solid inclusions in garnet. *Journal of Metamorphic Geology*, **30**, 193–212.
- Gerya, T., 2011. Future directions in subduction modeling. *Journal of Geodynamics*, **52**, 344–378.
- Gerya, T.V. & Meilick, F.I., 2011. Geodynamic regimes of subduction under an active margin: effects of rheological weakening by fluids and melts. *Journal of Metamorphic Geology*, **29**, 7–31.
- Gerya, T.V. & Yuen, D.A., 2003a. Characteristics-based marker-in-cell method with conservative finite-differences schemes for modelling geological flows with strongly variable transport properties. *Physics of the Earth and Planetary Interiors*, **140**, 295–318.
- Gerya, T.V. & Yuen, D.A., 2003b. Rayleigh-Taylor instabilities from hydration and melting propel “cold plumes” at subduction zones. *Earth and Planetary Science Letters*, **212**, 47–62.
- Gerya, T.V., Yuen, D.A. & Maresch, W.V., 2004a. Thermo-mechanical modeling of slab detachment. *Earth and Planetary Science Letters*, **226**, 101–116.
- Gerya, T.V., Yuen, D.A. & Sevre, E.O.D., 2004b. Dynamical causes for incipient magma chambers above slabs. *Geology*, **32**, 89–92.
- Gerya, T.V., Perchuk, L.L. & Burg, J.-P., 2008. Transient hot channels: perpetrating and regurgitating ultrahigh-pressure, high-temperature crust-mantle associations in collision belts. *Lithos*, **103**, 236–256.
- Gilotti, J. & McClelland, W.C., 2007. Characteristic of, and a tectonic model for, ultrahigh-pressure metamorphism in the Overriding plate of the Caledonian orogen. *International Geology Review*, **49**, 777–797.
- Gorczyk, W., Willner, A.P., Connolly, J.A.D. & Burg, J.-P., 2007. Physical controls of magmatic productivity at Pacific-type convergent margins: new insights from numerical modelling. *Physics of the Earth and Planetary Interiors*, **163**, 209–232.
- Grove, T.L., Chatterjee, N., Parman, S.W. & Medard, E., 2006. The influence of H<sub>2</sub>O on mantle wedge melting. *Earth and Planetary Science Letters*, **249**, 74–89.
- Hacker, B., Luffi, P., Lutkov, V. *et al.*, 2005. Near-ultrahigh pressure processing of continental crust: Miocene crustal xenoliths from the Pamir. *Journal of Petrology*, **46**, 1661–1687.
- Hacker, B.R., Andersen, T.B., Johnston, S. *et al.*, 2010. High-temperature deformation during continental-margin subduction and exhumation: the ultrahigh-pressure Western Gneiss Region of Norway. *Tectonophysics*, **480**, 149–171.
- Hacker, B.R., Kelemen, P.B. & Behn, M.D., 2011. Differentiation of the continental crust by reamination. *Earth and Planetary Science Letters*, **307**, 501–516.
- Hawkesworth, C.J., Turner, S.P., McDermott, F., Peate, D.W. & van Calsteren, P., 1997. U–Th isotopes in arc magmas: implications for element transfer from the subducted crust. *Science*, **276**, 551–555.
- Hermann, J. & Green, D.H., 2001. Experimental constraints on high pressure melting in subducted crust. *Earth and Planetary Science Letters*, **188**, 149–186.
- Hermann, J., Rubatto, D., Korsakov, A. & Shatsky, V.S., 2001. Multiple zircon growth during fast exhumation of diamondiferous, deeply subducted continental crust (Kokchetav Massif, Kazakhstan). *Contributions to Mineralogy and Petrology*, **141**, 66–82.
- Husson, L., Brun, J.-P., Yamato, P. & Faccenna, C., 2009. Episodic slab rollback fosters exhumation of HP–UHP rocks. *Geophysical Journal International*, **179**, 1292–1300.
- Kaneko, Y., Maruyama, S., Terabayashi, M. *et al.*, 2000. Geology of the Kokchetav UHP–HP metamorphic belt, Northern Kazakhstan. *The Island Arc*, **9**, 264–283.
- Labrousse, L., Jolivet, L., Agard, P., Hebert, R. & Anderson, T.B., 2002. Crustal scale boudinage and migmatization of gneiss during their exhumation in the UHP province of Western Norway. *Terra Nova*, **14**, 263–270.
- Labrousse, L., Prouteau, G. & Ganzhorn, A.-C., 2011. Continental exhumation triggered by partial melting at ultrahigh pressure. *Geology*, **39**, 1171–1174.
- Lang, H.M. & Gilotti, J.A., 2007. Partial melting of metapelites at ultrahigh-pressure conditions, Greenland Caledonides. *Journal of Metamorphic Geology*, **25**, 129–147.
- Li, Z. & Gerya, T., 2009. Polyphase formation and exhumation of high- to ultrahigh-pressure rocks in continental subduction zone: numerical modelling and application to the Sulu ultrahigh-pressure terrane in eastern China. *Journal of Geophysical Research*, **114**, article no.: B09406.
- Li, Z.H., Xu, Z.Q. & Gerya, T.V., 2011. Flat versus steep subduction: contrasting modes for the formation and exhumation of high- to ultrahigh-pressure rocks in continental collision zones. *Earth and Planetary Science Letters*, **301**, 65–77.
- Liou, J.G., Tsujimori, T., Zhang, R.Y., Katayama, I. & Maruyama, S., 2004. Global UHP metamorphism and continental subduction/collision: the Himalayan model. *International Geology Review*, **46**, 1–27.

- Little, T.A., Hacker, B.R., Gordon, S.M. *et al.*, 2011. Diapiric exhumation of Earth's youngest (UHP) eclogites in the gneiss domes of the D'Entrecasteaux Islands, Papua New Guinea. *Tectonophysics*, **510**, 39–68.
- Mancktelow, N.S., 1995. Nonlithostatic pressure during sediment subduction and development and exhumation of high-pressure metamorphic rocks. *Journal of Geophysical Research*, **100**, 571–583.
- Maruyama, S., Liou, J.G. & Terabayashi, M., 1996. Blueschists and eclogites of the world, and their exhumation. *International Geology Review*, **38**, 485–594.
- Massonne, H.J., 2003. A comparison of the evolution of diamondiferous quartz-rich rocks from the Saxonian Erzgebirge and the Kokchetav Massif: are so-called diamondiferous gneisses magmatic rocks? *Earth and Planetary Science Letters*, **216**, 347–364.
- Massonne, H.J., 2009. Hydration, dehydration, and melting of metamorphosed granitic and dioritic rocks at high- and ultrahigh-pressure conditions. *Earth and Planetary Science Letters*, **288**, 244–254.
- Mishin, Y.A., Gerya, T.V., Burg, J.-P. & Connolly, J.A.D., 2008. Dynamics of double subduction: numerical modeling. *Physics of the Earth and Planetary Interiors*, **171**, 280–295.
- Nie, S., Yin, A., Rowley, D.B. & Jin, Y., 1994. Exhumation of the Dabie Shan ultra-high-pressure rocks and accumulation of the Songpan-Ganzi flysch sequence, central China. *Geology*, **22**, 999–1002.
- Nikolaeva, K., Gerya, T.V. & Connolly, J.A.D., 2008. Numerical modelling of crustal growth in intraoceanic volcanic arcs. *Physics of the Earth and Planetary Interiors*, **171**, 336–356.
- Okay, A. & Sengör, A.M., 1992. Evidence for intracontinental thrust-related exhumation of the ultrahigh-pressure rocks in China. *Geology*, **20**, 411–414.
- Okay, A., Sengör, A.M. & Satir, M., 1993. Tectonics of an ultrahigh-pressure metamorphic terrane—the Dabie-Shan-Tongbai-shan orogen, China. *Tectonics*, **12**, 1320–1334.
- Parrish, R.R., Gough, S.J., Searle, M.P. & Waters, D.J., 2006. Plate velocity exhumation of ultrahigh-pressure eclogites in the Pakistan Himalaya. *Geology*, **34**, 989–992.
- Piffner, O.A., Ellis, S. & Beaumont, C., 2000. Collision tectonics in the Swiss Alps: insight from geodynamic modeling. *Tectonics*, **19**, 1064–1094.
- Ragozin, A.L., Liou, J.G., Shatsky, V.S. & Sobolev, N.V., 2009. The timing of the retrograde partial melting in the Kumdy-Kol region (Kokchetav Massif, Northern Kazakhstan). *Lithos*, **109**, 274–284.
- Ranalli, G., 1995. *Rheology of the Earth*. Chapman and Hall, London, 413 pp.
- Ratschbacher, L., Hacker, B.R., Webb, L.E. *et al.*, 2000. Exhumation of the ultrahigh-pressure continental crust in east central China: Cretaceous and Cenozoic unroofing and the Tan-Lu fault. *Journal of Geophysical Research – Solid Earth*, **105**, 13,303–13,338.
- Root, D.B., Hacker, B.R., Gans, P.B., Ducea, P.B., Eide, E.A. & Mosenfelder, J.L., 2005. Discrete ultrahigh-pressure domains in the Western Gneiss Region, Norway: implications for formation and exhumation. *Journal of Metamorphic Geology*, **23**, 45–61.
- Rubatto, D. & Hermann, J., 2001. Exhumation as fast as subduction? *Geology*, **29**, 3–6.
- Ryan, P.D., 2001. The role of deep basement during continent-continent collision. A review. In: *Continental Reactivation and Reworking* (eds Miller, J.A., Holdsworth, R.E., Buick, I.S. & Hand, M.). *Geological Society, London, Special Publication*, **184**, 39–55.
- Schmeling, H., Babeyko, A.Y., Enns, A. *et al.*, 2008. Benchmark comparison of spontaneous subduction models—towards a free surface. *Physics of the Earth and Planetary Interiors*, **171**, 198–223.
- Schmidt, S.M. & Kissling, E., 2000. The arc of the western Alps in the light of geophysical data on deep crustal structure. *Tectonics*, **19**, 62–85.
- Schmidt, M. & Poli, S., 1998. Experimentally based water budgets for dehydrating slabs and consequences for arc magma generation. *Earth and Planetary Letters*, **163**, 361–379.
- Sizova, E., Gerya, T., Brown, M. & Perchuk, L.L., 2010. Subduction styles in the Precambrian: insight from numerical experiments. *Lithos*, **116**, 209–229.
- Skjerlie, K.P. & Patino Douce, A.E., 2002. The fluid-absent partial melting of a zoisite-bearing quartz eclogite from 1.0 to 3.2 GPa: implication for melting in thickened continental crust and for subduction-zone processes. *Journal of Petrology*, **43**, 291–314.
- Smye, A.J., Greenwood, L.V. & Holland, T.J.B., 2010. Garnet-chloritoid-kyanite assemblages: eclogite facies indicators of orogenic constraints in orogenic belts. *Journal of Metamorphic Geology*, **28**, 753–768.
- Stoeckhert, B. & Gerya, T.V., 2005. Pre-collisional high pressure metamorphism and nappe tectonics at active continental margins: a numerical modelling simulation. *Terra Nova*, **17**, 102–110.
- Stoeckhert, B., Duyster, J., Trepmann, C. & Massonne, H.J., 2001. Microdiamond daughter crystals precipitated from supercritical COH silicate fluids included in garnet, Erzgebirge, Germany. *Geology*, **29**, 391–394.
- Toth, J. & Gurnis, M., 1998. Dynamics of subduction initiation at preexisting fault zones. *Journal of Geophysical Research – Solid Earth*, **103**, 18,053–18,067.
- Tsujimori, T., Sisson, V.B., Liou, J.G., Harlow, G.E. & Sorensen, S.S., 2006. Very-low-temperature record of the subduction process: a review of worldwide lawsonite eclogites. *Lithos*, **92**, 609–624.
- Turcotte, D.L. & Schubert, G., 2002. *Geodynamics*. Cambridge University Press, Cambridge, 456 pp.
- van den Beukel, J., 1992. Some thermomechanical aspect of the subduction of continental lithosphere. *Tectonics*, **11**, 316–329.
- Vance, D., Bickle, M., Ivy-Ochs, S. & Kubik, P.W., 2003. Erosion and exhumation in the Himalaya from cosmogenic isotope inventories of river sediments. *Earth and Planetary Science Letters*, **206**, 273–288.
- Vrijmoed, J.C., Podladchikov, Y.Y., Andersen, T.B. & Hartz, E.H., 2009. An alternative model for ultra-high pressure in the Svartberget Fe-Ti garnet-peridotite, Western Gneiss Region, Norway. *European Journal of Mineralogy*, **21**, 1119–1133.
- Wallis, S., Tsuboi, M., Suzuki, K., Fanning, M., Jiang, L. & Tanaka, T., 2005. Role of partial melting in the evolution of the Sulu (eastern China) ultrahigh-pressure terrane. *Geology*, **33**, 129–132.
- Wang, Q.C. & Cong, B.L., 1999. Exhumation of UHP terranes: a case study from the Dabie Mountains, eastern China. *International Geology Review*, **41**, 994–1004.
- Wang, Q., Liu, X. & Wu, W., 1997. Intrusive contact between granitic gneiss and UHP rocks: evidence from the Chinese Dabie Mountains and tectonic implications [abs.]: Fifth International Eclogite Conference. *Terra Nova*, **9**, 40.
- Warren, C.J., Beaumont, C. & Jamieson, R., 2008a. Deep subduction and rapid exhumation: role of crustal strength and strain weakening in continental subduction and ultrahigh-pressure rock exhumation. *Tectonics*, **27**, article no.: TC6002.
- Warren, C.J., Beaumont, C. & Jamieson, R., 2008b. Modelling tectonic styles and ultra-high pressure (UHP) rock exhumation during the transition from oceanic subduction to continental collision. *Earth and Planetary Science Letters*, **267**, 129–145.
- Wittmann, H., von Blanckenburg, F., Kruesmann, T., Norton, K.P. & Kubik, P.W., 2007. Relation between rock uplift and denudation from cosmogenic nuclides in river sediment in the Central Alps of Switzerland. *Journal of Geophysical Research*, **112**, 1–20.
- Xu, Z., Zeng, L., Liu, F. *et al.*, 2006. Polyphase subduction and exhumation of the Sulu high-pressure-ultrahigh-pressure metamorphic terrane. *Geological Society of America Special Papers*, **403**, 93–113.
- Yamato, P.E., Burrov, E., Agart, P., Le Pourhiet, L. & Jolivet, L., 2008. HP-UHP exhumation during slow continental subduc-

- tion: self-consistent thermodynamically and thermomechanically coupled model with application to the Western Alps. *Earth Planetary Science Letters*, **271**, 63–74.
- Yin, A. & Nie, S.Y., 1993. Development of the Tan-Lu fault as a transform system collision of the north and south China blocks, east-central China. *Tectonics*, **12**, 801–813.
- Yin, A., Manning, C.E., Lovera, O., Menold, C.A., Chen, X. & Gehrels, G.E., 2007. Early Paleozoic tectonic and thermomechanical evolution of ultrahigh-pressure (UHP) metamorphic rocks in the Northern Tibetan plateau, Northwest China. *International Geology Review*, **49**, 681–716.
- Zeng, L.S., Liang, F.H., Asimow, P., Chen, F.Y. & Chen, J., 2009. Partial melting of deeply subducted continental crust and the formation of quartzofeldspathic polyphase inclusions in the Sulu UHP eclogites. *Chinese Science Bulletin*, **54**, 2,580–2,594.
- Zheng, Y.-F., Xia, Q.-X., Chen, R.-X. & Gao, X.-Y., 2011. Partial melting, fluid supercriticality and element mobility in ultrahigh-pressure metamorphic rocks during continental collision. *Earth-Science Reviews*, **107**, 342–374.
- Zhong, Z., Suo, S., You, Z. & Zhang, H., 2001. Major constituents of the Dabie collisional orogenic belt and partial melting in the ultrahigh-pressure unit. *International Geology Review*, **43**, 226–236.
- Zhu, G., Gerya, T.V., Yuen, D.A., Honda, S., Yoshida, T. & Connolly, J.A.D., 2009. 3-D Dynamics of hydrous thermal-chemical plumes in oceanic subduction zones. *Geochemistry, Geophysics, Geosystems*, **10**, article no.: Q11006.

## SUPPORTING INFORMATION

Additional Supporting Information may be found in the online version of this article:

**Appendix S1.** Description of the numerical model.

Please note: Wiley-Blackwell are not responsible for the content or functionality of any supporting materials supplied by the authors. Any queries (other than missing material) should be directed to the corresponding author for the article.

*Received 16 January 2012; revision accepted 16 July 2012.*